Chapter 4

Results and Discussion

4. Results and Discussion

This Chapter presents experimental results obtained from the studies related to the treatment of diesel contaminated soil by surfactant foam stabilized by different systems and corresponding analysis.

4.1 Remediation of diesel contaminated Soil

4.1.1 Remediation of diesel contaminated soil by Tween-80 and SDS foam stabilized with Allyl alcohol and Ethylene glycol

Surface Tension

Fig. 4.1 shows the variation of surface tension of 2 wt% of SDS and 0.2 vol% Tween-80 aqueous solutions prepared with different concentration of ethylene glycol and allyl alcohol additives. As a general trend, a sharp decrease is observed initially with the addition of additives for both the surfactant (0.2 wt% SDS and 0.2 vol% Tween-80). With Further raise in concentration, allyl alcohol tends to reduce the surface tension of solution, whereas solutions with ethylene glycol show an increasing trend . Allyl alcohol (5 mg/l) produces minimum surface tension values of 53.7 and 51.3 mN/m for SDS and Tween-80 solutions, respectively. For ethylene glycol the maximum surface tension of 71.2 and 62.9 mN/m are obtained for SDS and Tween-80 solutions, respectively. These are in accordance with results previously reported in the literature (Glenn et al., 2005). For the aqueous solution of the surfactants, such as Tween-40, 60, and 80, an increasing trend in surface tension values with increasing concentration of ethylene glycol is observed. This phenomenon can be explained based on the fact that the formation of micelles is influenced by the interaction of polar head group of the surfactant molecules with solvents. The polar polyoxyethylene head groups of the Tweens remain solubilized by formation of hydrogen bond by dipolar interaction with water. Thus ethylene glycol acts as a bond breaker

and affects the surface tension negatively (Carnero Ruiz and Aguiar, 2008; Nagarajan and Wang, 1996). However, the mechanism underlining the effect of allyl alcohol on the surface tension remains unclear.

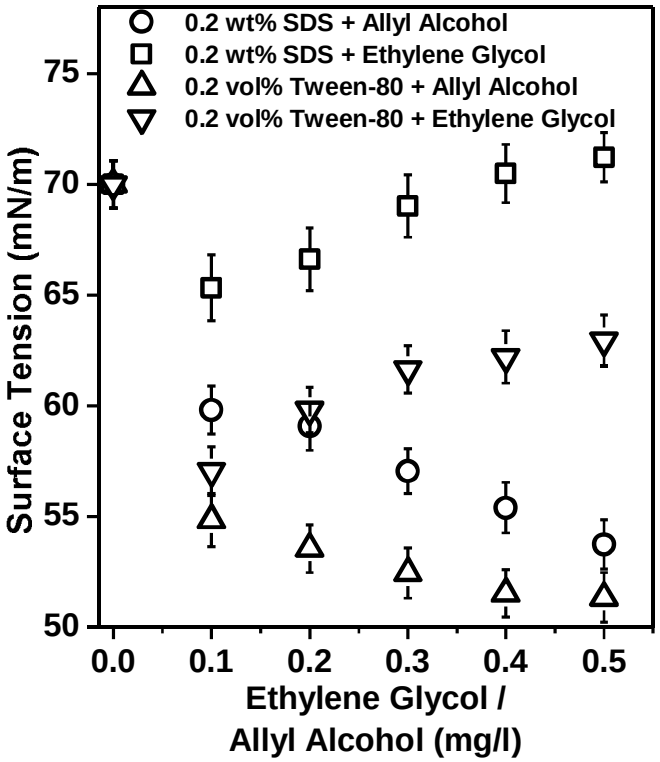

Fig. 4.1 Variation of surface tension of 0.02 wt% of SDS and 0.2 vol% Tween-80 aqueous solutions prepared with different concentration of ethylene glycol and allyl alcohol additives

Foamability

The effect of allyl alcohol Fig. 4.2 (a) and ethylene glycol Fig. 4.2 (b) on the foamability of SDS and Tween-80 are compared prior to the remediation of soil. For the solution with surfactant Tween-80 and maximum alcohol concentration of 3 mg/l, allyl alcohol shows higher foamability in terms of maximum foam volume compared to that of the ethylene glycol. The maximum MFV of 171 and 168 mL is observed for the 0.2 vol% surfactant Tween-80 foam stabilized by 3 mg/l allyl alcohol and ethylene glycol, respectively. For the anionic surfactant SDS, the MFV measures to be 165 mL for both ethylene glycol and allyl alcohol, used at the concentration of 2 mg/l. The results obtained are found to be in accordance with that of existing

literature (Fujii et al., 2006; Jackson et al., 1980). Reportedly, in the presence of allyl alcohol along SDS produces a higher volume of foam or foamability compared to that of Tween-80 (Azira et al., 2008; Mulligan and Eftekhari, 2003).

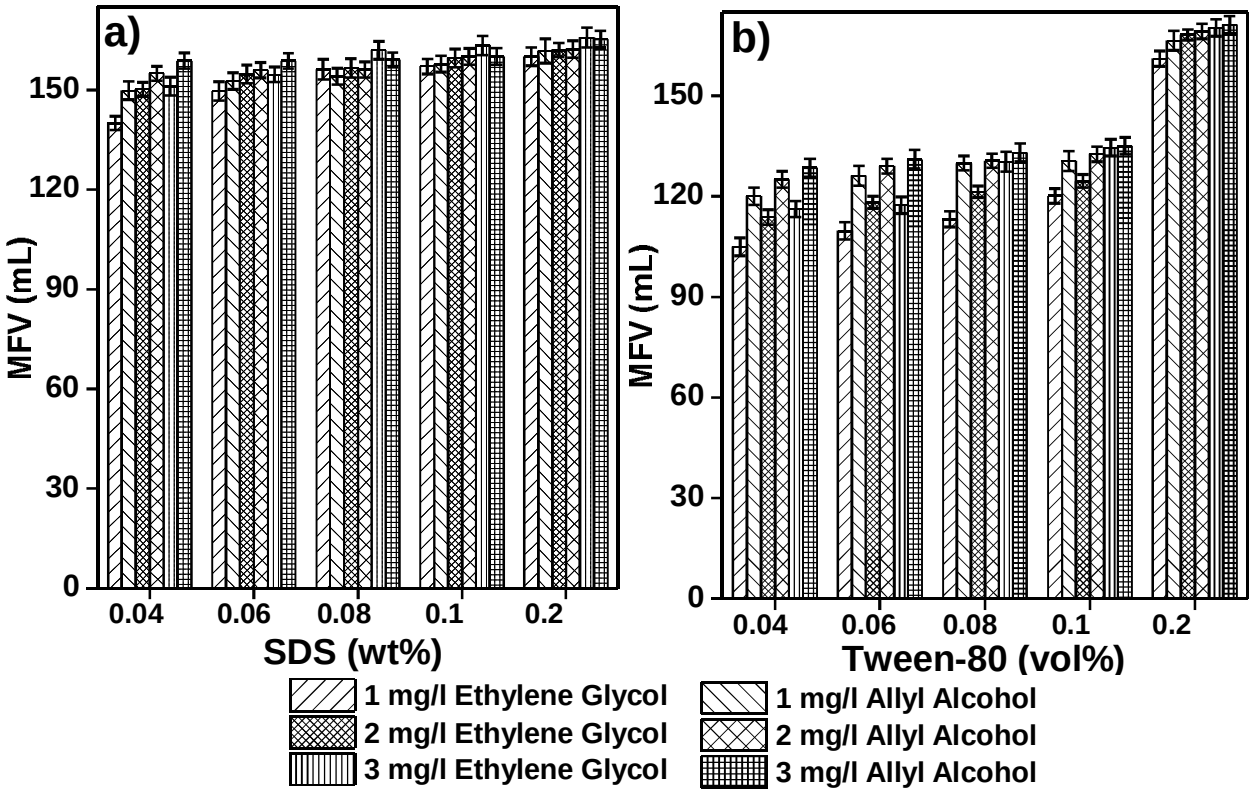

Fig. 4.2 Comparison of foamability (MFV) of ethylene glycol and allyl alcohol (1, 2, 3 mg/l) stabilized surfactant foam at varying concentrations of (a) SDS and (b) Tween-80.

Foam stability

The key factor in achieving stable foam is to overcome the destabilizing mechanism, such as drainage of liquid, coarsening, and coalescence of bubbles. The combination of additives such as polymers, alcohols, nanoparticles along with surfactants may influence the foam characteristics and stability to a great extent (Xiao et al., 2017). The stability of the foam produced by a mixture of surfactants and additives such as allyl alcohol and ethylene glycol is measured in terms of half-life, as shown in Fig. 4.3. As a general trend, the foam produces by Tween 80 remain stable

for a longer duration than that of SDS. The surfactant foam remains stable for a longer period after adding allyl alcohol than that for the ethylene glycol foams. The foams produce by 0.2 vol% of Tween 80 with ethylene glycol (3 mg/l), and allyl alcohol (3 mg/l) demonstrate a half-life of 16 and 18 min, respectively. In case of SDS (0.2 wt%) the foam produce by allyl alcohol and ethylene glycol (3 mg/l) show a half-life of 14 and 9 min, respectively. Even the lowest concentration of allyl alcohol (1 mg/l) results in foam of higher stability compared to that of the ethylene glycol (1 mg/l) with the same amount of surfactant used. For example, 1 mg/l allyl alcohol along with 0.2 vol% of Tween 80 resulted in foam that has a half-life of 16 min. However, ethylene glycol (1 mg/l) with the same amount of surfactant Tween 80 (0.2 vol%) produces foam that has a half-life of 12 min.

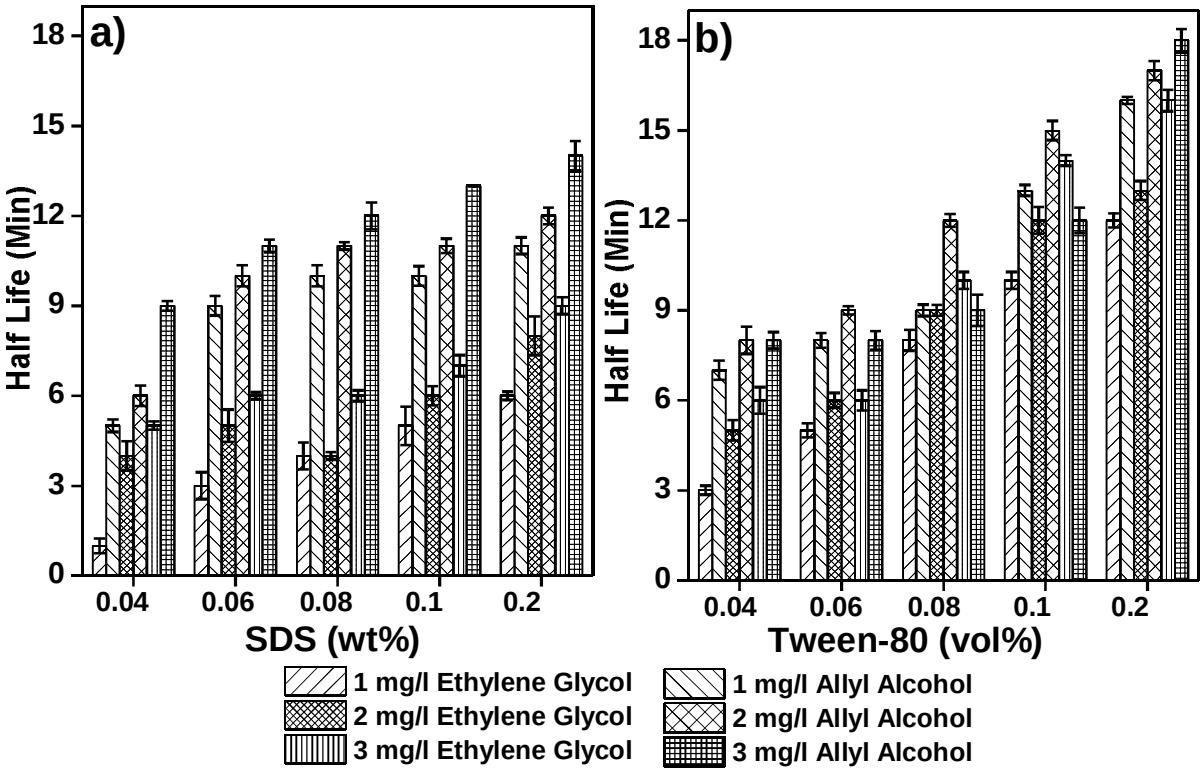

Fig. 4.3 Effect of varying concentrations of ethylene glycol and allyl alcohol on the half-life of the foam produced with different concentrations surfactants (a) SDS and (b) Tween-80.

Stable Foam in the removal of diesel oil from contaminated soil

Figs. 4.4 (a) and (b) show the diesel oil removal efficiency (%)from contaminated soil by aqueous foams of surfactant SDS and Tween 80 stabilized by ethylene glycol and allyl alcohol, respectively. From the plot, it can be observed that the removal efficiency increases with increase in surfactant concentration, in general. Also, the nonionic surfactant Tween-80 yields higher removal efficiency than the anionic surfactant SDS in combination with allyl alcohol. 0.2 wt% SDS aqueous solution along with 3 mg/l of allyl alcohol and ethylene glycol results in 62 and 57.5 % of diesel removal efficiency, respectively (Fig.4.4a). The maximum diesel removal efficiency of 71.5 % is achieved for 0.2 vol% of Tween 80 along with 3 mg/l of allyl alcohol, whereas the ethylene glycol produces 63 % at the same condition.

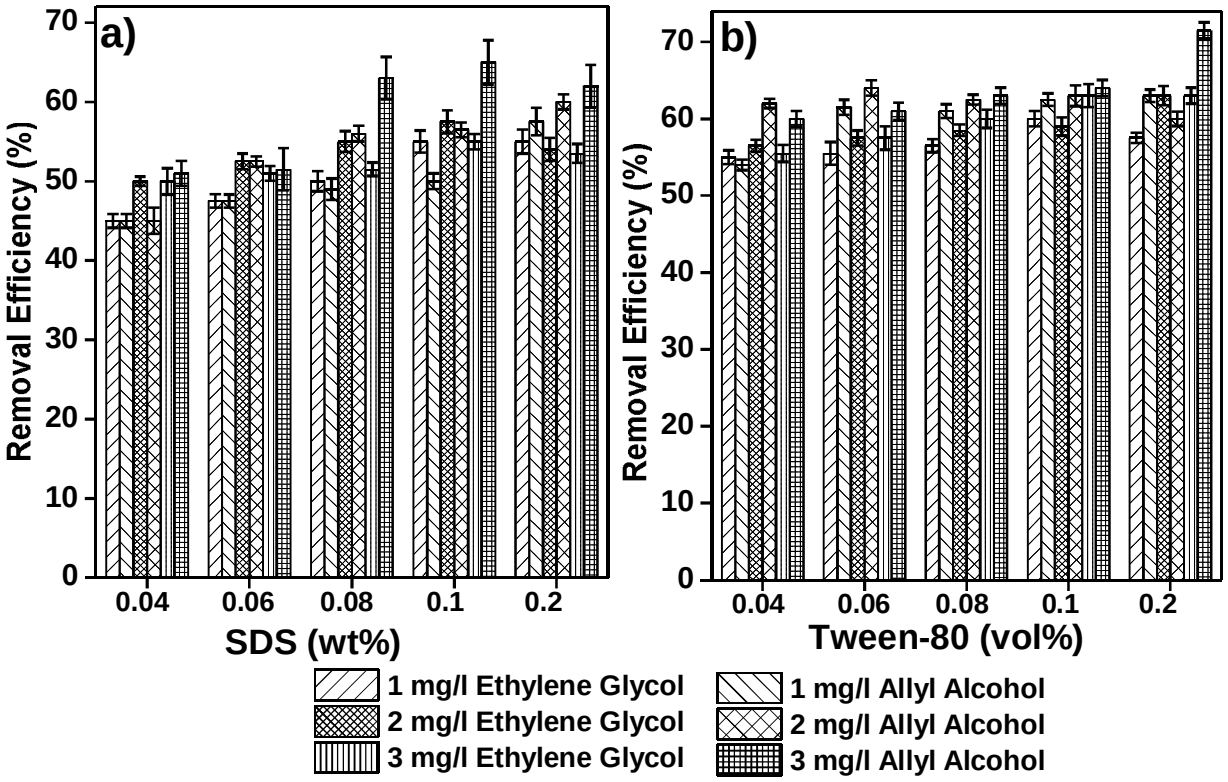

Fig. 4.4 Efficiency (%) of diesel oil removal from contaminated soil by using aqueous foam prepared from various concentrations of (a) SDS and (b) Tween-80 and stabilized by ethylene glycol and allyl alcohol of different concentration.

Adsorption of surfactant to soil

Only the nonionic surfactant Tween-80, which produces higher soil remediation effect than the anionic surfactant SDS, is considered for the adsorption studies. The experimental data obtained for adsorption is fitted to the Freundlich and Langmuir isotherm equations. Langmuir and Freundlich isotherms are the most commonly used isotherms for depicting the mechanism of adsorption of surfactant onto the soil. In these equations (Table 4.1), C_e represents the equilibrium concentration of the surfactant, q_e represents the adsorption capacity, q_m is the theoretical maximum adsorption capacity, K_L & K_f are the Langmuir and Freundlich constants, respectively and n is the heterogeneity constant (Qi et al., 2016; Rosas et al., 2013). Table 4.1 shows the values of R^2 for different adsorption models, and it is found that the Langmuir model exhibited a better R^2 value of 0.9686. The results depict that initially, the absorptivity of Tween 80 in the soil increases with the increase in equilibrium concentrations of surfactant. The 'n' value obtained using the Freundlich model is greater than one. A similar result has been described by other researchers (Brownawell et al., 1997; Rodríguez-Cruz et al., 2005). (Brownawell et al., 1997) compares the adsorption behavior of the nonionic, anionic and cationic surfactant. The surfactant adsorption is strongest for the cationic and weakest for the anionic surfactant, but the nonionic surfactant has adsorption in-between these two owing to the negative affinity of the soil.

Table 4.1: Parameters obtained for Freundlich and Langmuir model equations for adsorption of nonionic surfactant Tween-80 onto the soil

Adsorption Model	**Equation**	**R^2 Value**	**Parameters**	
Langmuir Model	$C_e/q_e = 1/K_L + C_e/q_m$	0.9686	K_L= 0.1452	qm= 12.4
Freundlich Model	$\ln(q_e) = \ln(K_f) + 1/n \ln(C_e)$	0. 9247	K_F = 1.6236	*n* = 1.7

The maximum diesel removal efficiency achieved by the Tween-80 foam stabilized with biodegradable additive Allyl alcohol is 71.5 %. Now, with an aim to achieve better contaminant removal efficiency from the soil we focus to use nanoparticles in combination with different surfactants to stabilize aqueous foam. For this we have selected the combinations of silica (hydrophilic & hydrophobic SiO_2) along with nonionic surfactant Tween-20 in one study and iron nanoparticles (Fe^0 & Fe_3O_4) along with nonionic surfactant APG-Ph in another study. In the following sections we report the results obtained for the selected combinations of nanoparticles and surfactants in terms of foam properties and diesel removal efficiency from soil.

4.1.2 Remediation of diesel contaminated soil by Tween-20 foam stabilized with silica nanoparticle

Surface Tension

Fig. 4.5 illustrates the surface tension results for aqueous Tween-20 solutions, and dispersions of Tween-20 stabilized with hydrophilic and hydrophobic SiO_2 nanoparticles at various concentrations of the surfactant. The surface tension provides an understanding of the adsorption behavior of surfactant on different types of nanoparticles, which affects foam properties (Yazhgur et al., 2013b). A general reduction in surface tension with increase in surfactant concentration is observed for the pure dispersion, and both the hydrophobic and hydrophilic SiO_2 nanoparticle stabilized dispersions. The surface tension of the pure Tween-20 dispersion at the lowest concentration of 0.02 vol% is 69.6 mN/m. The same dispersion shows a significant decrease in surface tension with addition of hydrophilic (59.6 mN/m) and hydrophobic (56.9 mN/m) SiO_2 particles. The surface tension of the maximum concentration of pure Tween-20 dispersion (0.1 vol%) is 35.987 mN/m. However, with addition of 5 mg/l hydrophilic and hydrophobic SiO_2 nanoparticles, surface tension value reduces to 35.84 and 33.2 mN/m, respectively. The surface tension of Tween-20 solution data is in reasonable agreement with the existing literature (Kothekar et al., 2007).

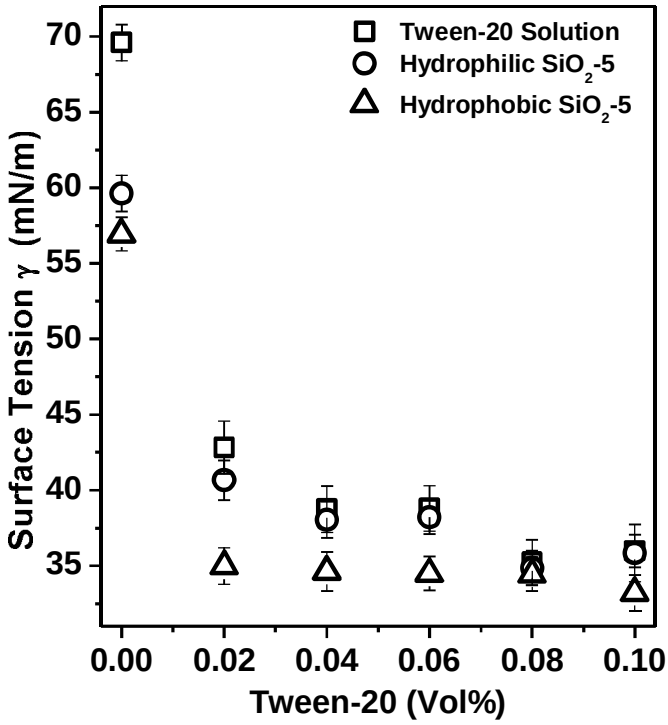

Fig. 4.5 Comparison of surface Tension (γ) values of aqueous Tween-20 solution and dispersions of Tween-20 stabilized with 5 mg/l hydrophilic SiO_2 and hydrophobic SiO_2.

Foamability and Foam stability

The comparisons of foamability and foam stability of the pure aqueous Tween-20 surfactant solution and surfactant solutions stabilized with varying concentrations of hydrophilic and hydrophobic SiO_2 nanoparticles are shown in Figs. 4.6 (a) and (b) and Figs. 4.6 (c) and (d), respectively. From the plot, it can be observed that the MFV and RMI 30 values increase with the increase in surfactant concentration and SiO_2 nanoparticles. However, it is more distinct for the solutions with hydrophobic SiO_2 nanoparticles than those with hydrophilic nanoparticles. For the pure Tween-20 surfactant solution the highest MFV and RMI 30 of 92.3 and 86.6 mL, respectively are obtained at the maximum concentration of 0.1 vol%. Hydrophobic SiO_2 nanoparticle (5 mg/l) causes the highest foamability and foam stability values of 115.6 and 117 mL, respectively, for 0.1 vol% Tween-20 solution. Whereas hydrophilic SiO_2 particles (5 mg/l) results in the highest MFV and RMI 30 values of 109.9 and 105.5 mL, respectively, for 0.1 vol%

Tween-20 solution. In comparison to the pure surfactant solution there are 25.2 and 35.1% increase in MFV and RMI 30, respectively, with the addition of hydrophobic SiO_2 nanoparticle. Similarly, there is 17.6 and 19.5 % increase in MFV and RMI 30, respectively, with the addition of hydrophilic SiO_2 nanoparticle. The foamability data with respect to hydrophobic SiO_2 nanoparticle dispersion is similar to the results found in the literature source. (Blute et al., 2007) report an increase in foamability with increase in hydrophobic SiO_2 nanoparticle concentration (1-15 %) and mention that the foamability is predominantly controlled by the hydrophobicity of nanoparticles. The transient foam is generated by dynamic foaming method by continuous sparging of nitrogen gas (1-8 mL/s) into the 10-15 mL of a surfactant-free aqueous dispersion containing commercially available hydrophobic and hydrophilic colloidal silica dispersion Bindzil CC30 and Nyacol 2034DI, respectively, prepared in 0.01 M NaCl solution. The foam height is recorded at each gas flow interval for the gas flow rates adequate to produce foam (foamability). Maximum foamability of 40 and 20 mL is observed at 8 mL/s for the 10 wt% Bindizin CC30 (7 nm) and Nyacol 2034DI (20 nm), respectively. Similarly with increase in the gas flow rate (1-8 mL/s) the foam volume is reported to increase for both hydrophobic and hydrophilic particles but, the hydrophobic particle (Bindzil) produces higher foam than the hydrophilic silica nanoparticles, indicating that the surface hydrophobicity of nanoparticles is well known to be a major parameter affecting the foaming systems. In the present study, varying concentrations of Tween-20 foam stabilized by 5 mg/l hydrophobic & hydrophilic SiO_2 which produced the maximum foamability and foam stability are further used in the soil remediation study.

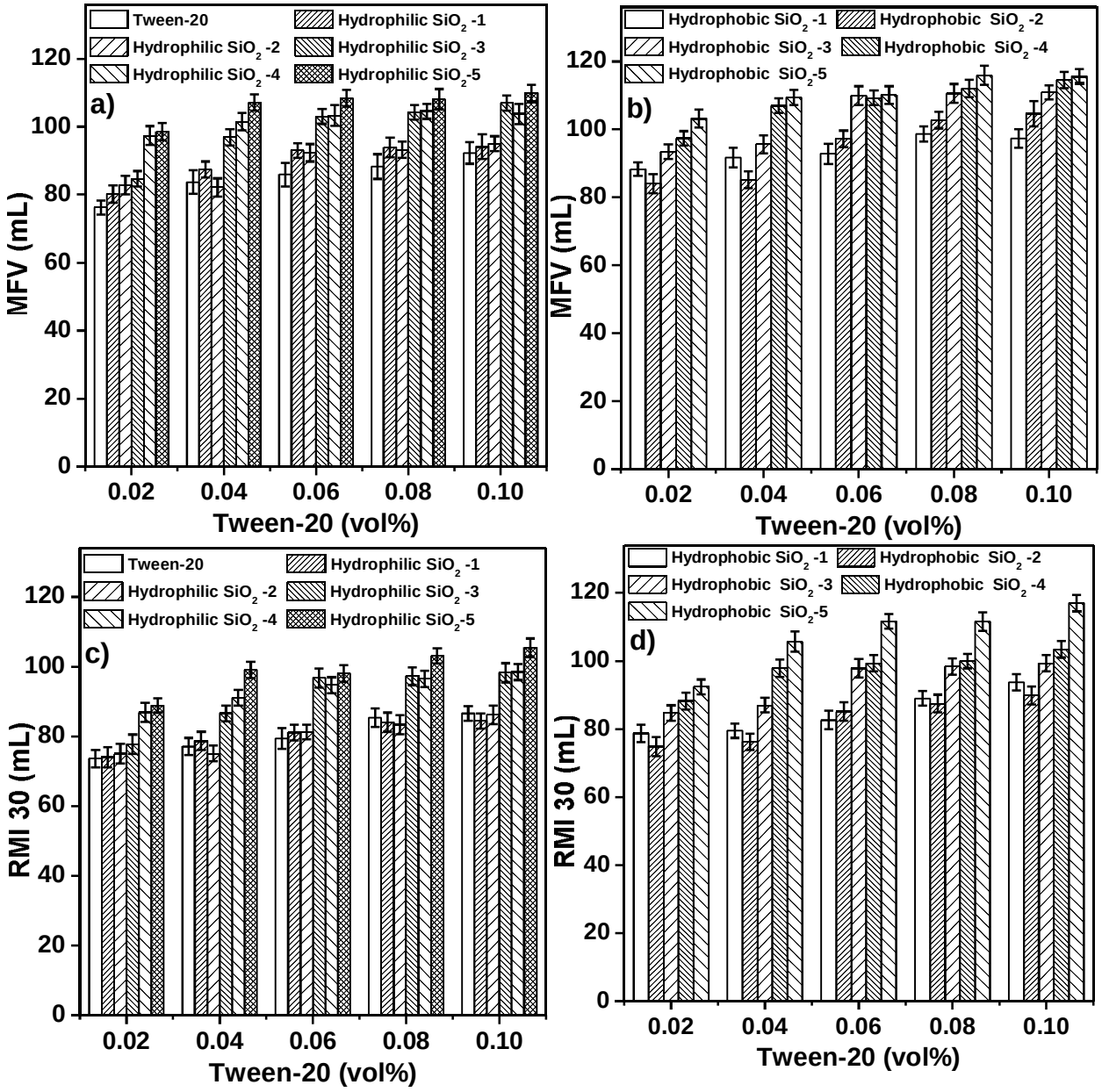

Fig. 4.6 Comparison of foamability (MFV) (a) and (b) and foam stability (RMI 30) (c) and (d) for different concentration of aqueous Tween-20 solutions (vol %) stabilized with different concentration of hydrophilic and hydrophobic SiO_2 nanoparticles, respectively.

Dynamic Foam Properties

Fig. 4.7 (a) depicts the change of dynamic foam volume with time for pure 0.1 vol% aqueous Tween-20 dispersion, and the same dispersion stabilized with 5 mg/l hydrophobic and hydrophilic SiO_2 nanoparticles. The dynamic change in volume of foam, produced by passing air at a flow rate of 5 mL/s, is plotted over a time period of 900 s. Nanoparticles, being a good foam stabilizer, tend to form a stable foam volume over a time period (Bournival and Ata, 2015). Surfactant solution with hydrophobic nanoparticle produces larger foam volume than the pure surfactant solution and surfactant solution with hydrophilic nanoparticle. This is because, in the case of the hydrophobic silica nanoparticle, the introduction of the hydrophobic groups causes a decrease in the surface tension free energy enabling the particles to become attached to the interface. This further leads us to decide that surfactant solution with nanoparticles can be used to remediate soil since stable foam aids better in the removal of contaminants from soil.

The effect of nanoparticle on foam drainage is further investigated to describe the foam stability. Generally, foam drainage is a phenomenon by which the liquid content in the foam drains by the effect of gravity. Not all the liquid from the foam could drain out due to capillary holdup until an equilibrium is reached (Gauchet et al., 2015). The drainage pattern exhibited by the foams prepared with 5 mg/l hydrophilic and hydrophobic SiO_2 nanoparticles with 0.1 vol% Tween-20 and 0.1vol% pure Tween-20 solution is shown in Fig. 4.7 (b). The volume of liquid drained increases initially and then remains constant (Saint-Jalmes, 2006). The liquid, from the foam created only with aqueous surfactant solution, tends to drain faster. At the end of 900 s, the 36.4, 37.6, and 38.8 ml of liquid drainage occur from 0.1 vol% Tween-20 foam stabilized by pure surfactant alone, 5 mg/l hydrophilic, and hydrophobic silica nanoparticles, respectively. In the present study the drainage of liquid from the foam stabilized by the 5 mg/l of hydrophobic silica

nanoparticles is found to be slowest. Though the mechanism by which hydrophobic particle affects foam drainage is unclear, the hydrophobic particles may adhere to the gas-liquid interface of the bubble retaining the liquid by acting as a barrier to prevent bubble breakage (Wang et al., 2016).

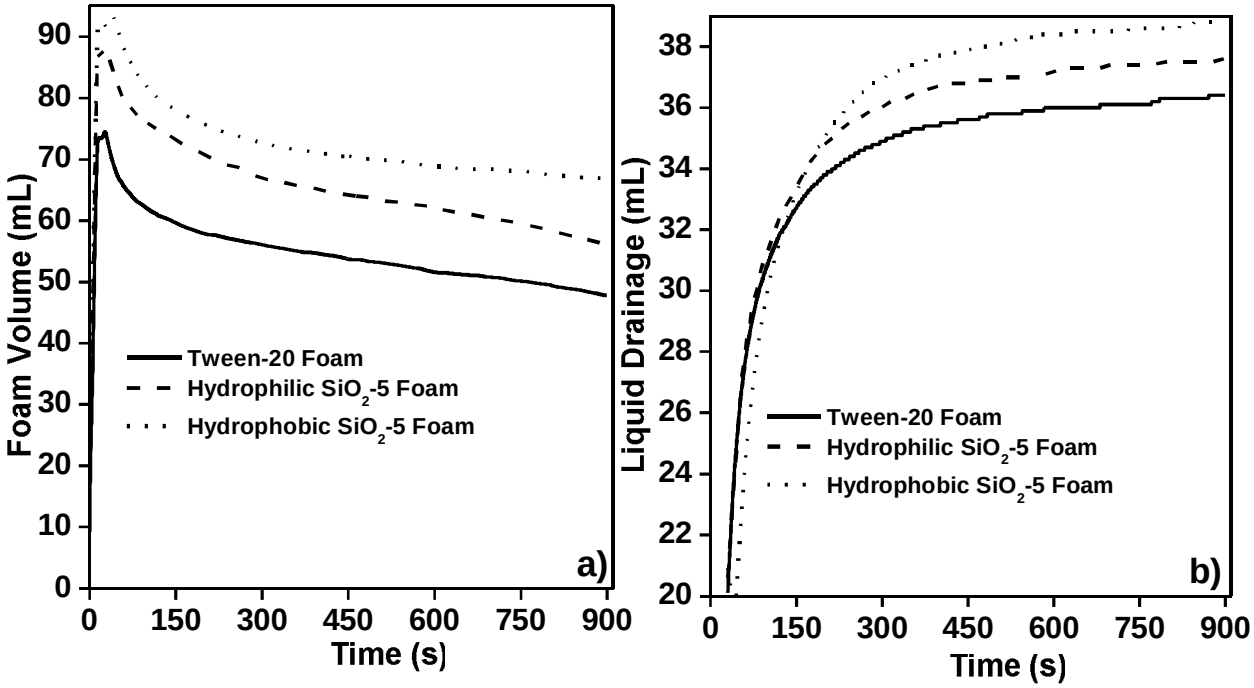

Fig. 4.7 Dynamic change in a) volume of foam and b) volume of liquid drained from the foam, generated using 0.1 vol% Tween-20 and 5 mg/l of hydrophilic and hydrophobic SiO_2 nanoparticle, with time.

Soil remediation studies

With the intention to enhance the diesel oil removal efficiency from contaminated desert soil, the soil is treated with pure surfactant solution, aqueous dispersion of SiO_2 nanoparticle, surfactant foam, and surfactant foam stabilized with nanoparticles in different experiments. With the increase in surfactant concentration, the diesel removal efficiency increases, and the maximum efficiency is observed with the foam stabilized by SiO_2 nanoparticles. The comparisons of efficiency (%) using pure Tween-20 surfactant solution, Tween-20 foam, and Tween-20 foams stabilized with 5 mg/l of SiO_2 hydrophilic and hydrophobic nanoparticles is

shown in Fig. 4.8. The 0.1 vol% pure Tween-20 solution and 0.1 vol% Tween-20 foam show 17.5 and 37.5 % diesel removal efficiency, respectively. The addition of SiO_2 nanoparticles helps to increase diesel oil removal efficiency to a certain level. The 0.1 vol% Tween-20 solution with 5 mg/l hydrophilic SiO_2 nanoparticle results in mere 29.5 % diesel removal. However, the 5 mg/l hydrophobic SiO_2 nanoparticle shows 42% diesel oil removal at the same surfactant concentration. The maximum diesel removal efficiency is achieved by the Tween-20 foam stabilized with 5 mg/l hydrophobic SiO_2 nanoparticle (78%), while the maximum removal efficiency obtained by the foam stabilized with hydrophilic nanoparticles is only 57.5%.

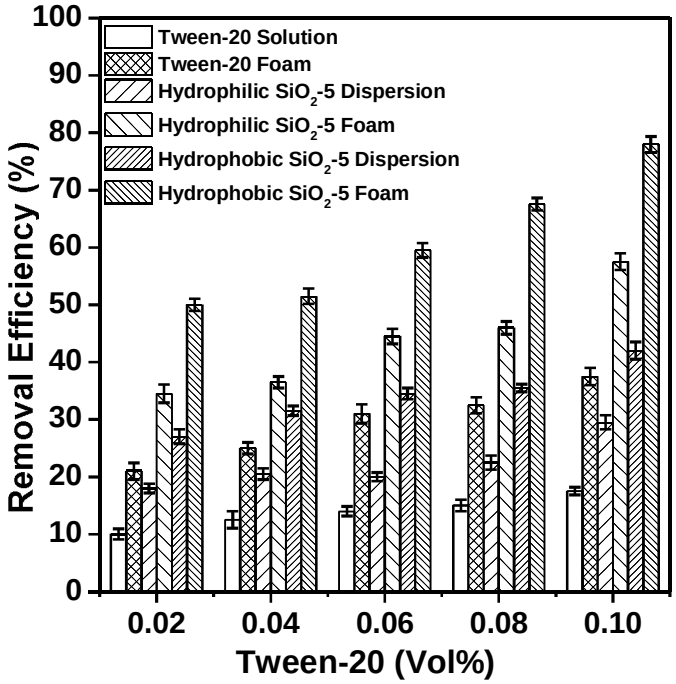

Fig. 4.8 Comparison of diesel oil removal efficiency from contaminated soil at varying concentration of Tween-20 (0.02-0.1 vol%): aqueous Tween-20 solution, Tween-20 foam, 5 mg/l dispersion of hydrophilic, hydrophobic SiO_2 nanoparticle and Tween-20 foams stabilized by 5 mg/l hydrophilic and hydrophobic SiO_2nanoparticle.

4.1.3 Remediation of diesel contaminated soil by APG-Ph foam stabilized with iron and oxide nanopowders

Physicochemical characteristics of iron and oxide nanomaterial

Figs. 4.9 (a) and (b) show the θ-2θ XRD spectra of the freshly prepared zero-valent iron and iron oxide powders, respectively. The oxide powder could be indexed as phase pure, polycrystalline, cubic magnetite (Fe_3O_4; JCPDS 11-614). The iron powder exhibits the presence of body-centered cubic crystalline zero-valent iron phase (Fe^0; JCPDS 06-0696) with some secondary phase (Fe_3O_4) corresponding to diffraction peak (311) at 35.42°. This Fe_3O_4 could be attributed to the presence of dissolved oxygen in solvents used during preparation. A similar observation has been reported by (Krzisnik et al., 2014) where Fe^0 powder synthesized by a liquid-phase reduction method has resulted in Fe^0 nanoparticles (~ 50 nm) with some FeO phase. The average crystallite size (D) of the powders is determined by Scherrer's equation: -(Zenou and Bakardjieva, 2018)

$$D=\frac{0.9\,\lambda}{\beta\cos\theta} \tag{19}$$

where λ is the wavelength of X-ray (1.54 Å) probe, β is the full width at half maximum intensity (FWHM), and θ corresponds to the maximum intensity position of the 100% XRD peak, (311) for Fe_3O_4 and (110) for Fe^0. The crystallite size for Fe_3O_4 and Fe^0 is calculated to be ~18 and ~28 nm, respectively.

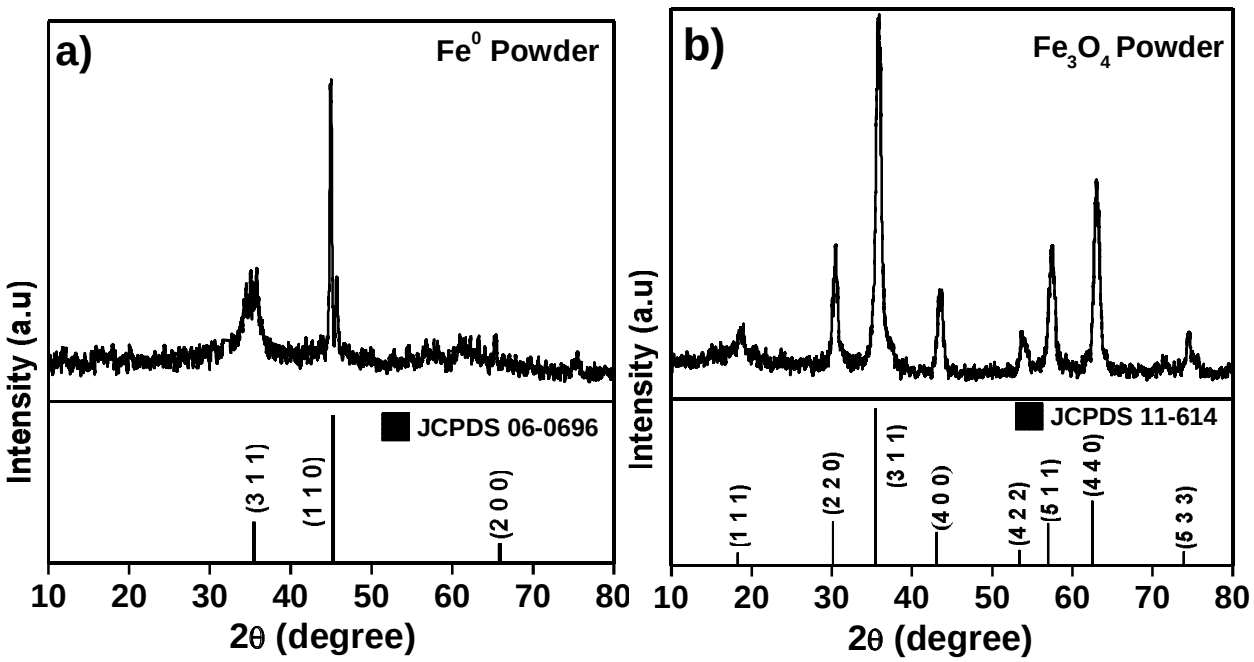

Fig. 4.9 XRD spectra of the freshly synthesized (a) Fe^0 and (b) Fe_3O_4 nanoparticles. The black bars at the bottom panels are the corresponding powder diffraction file data.

Figs. 4.10 (a) and (b) reveal the FESEM images of the Fe^0 and Fe_3O_4 powders. EDX (inset of Figs. 4.10 (a) and (b)) images of the nanoparticles indicate the presence of Fe and O in both the powders. For Fe_3O_4, the atomic % of Fe and O are close to the theoretical values; ~45 and 55 at%, respectively. For Fe^0, ~ 10 atomic % O is detected (Lominchar et al., 2018). The carbon peak for the Fe_3O_4 sample arises due to the carbon tape used to mount the sample during analysis. The particle size distribution (inset images of Figs. 4.10 (a) and (b) calculated from FESEM micrographs ranges between 5-60 nm (average ~ 20 nm) and 0-50 nm (average ~ 28 nm) for Fe^0 and Fe_3O_4, respectively. The equiaxed morphology of the synthesized Fe^0 and Fe_3O_4 nanopowders is clear from plan view TEM micrographs (Figs. 4.10 (c) and (d). The particle size distribution (inset images of Figs. 4.10 (c) and (d)) calculated from TEM micrographs ranges between 4-80 nm (average ~ 15 nm) and 1-80 nm (average ~20 nm) for Fe_3O_4 and Fe^0 samples,

respectively. These size distributions correspond to that of the crystallite size calculated using XRD data.

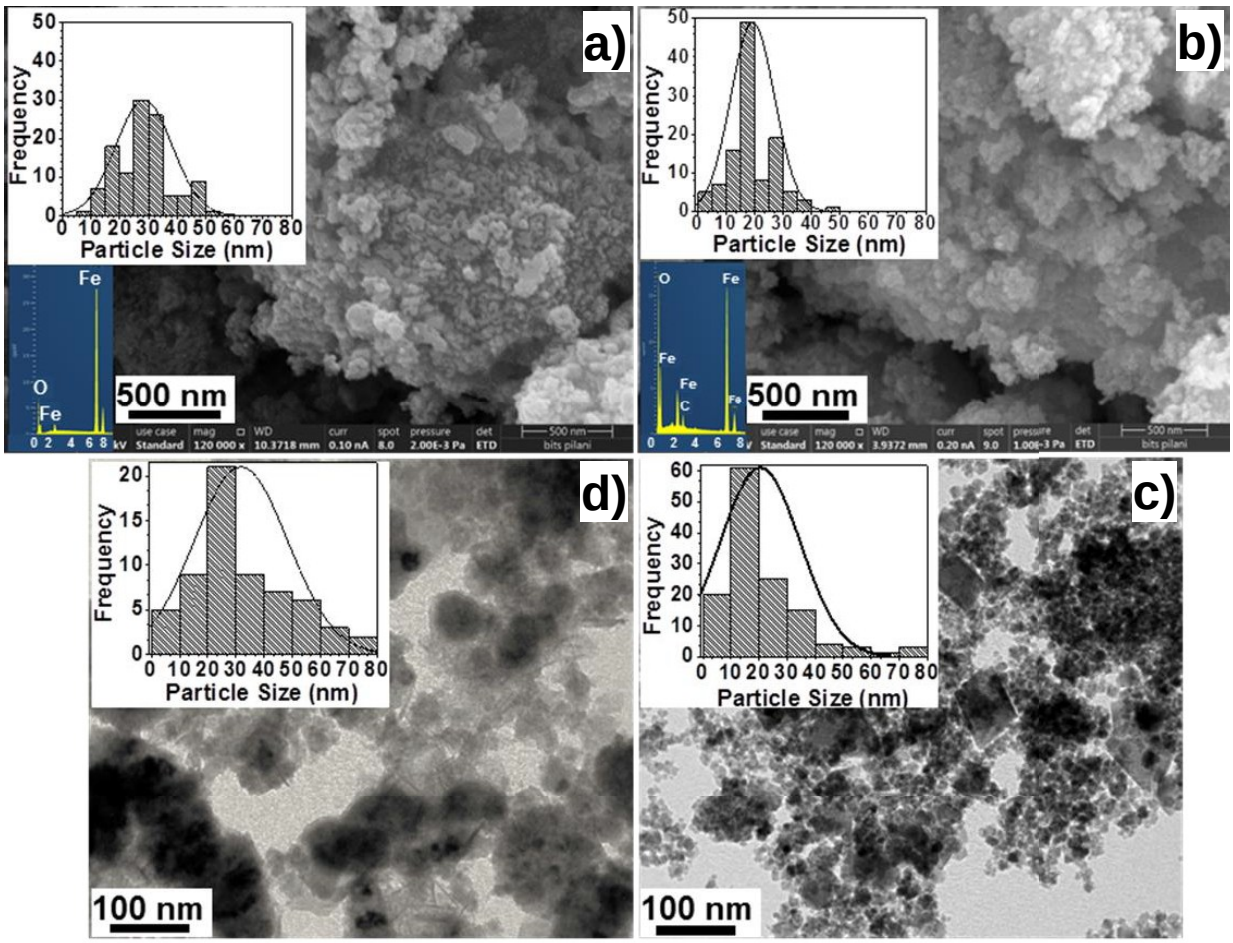

Fig. 4.10 SEM micrographs of (a) Fe^0 and (b) Fe_3O_4 nanoparticles at 120000X magnification along with particle size distribution and EDS analysis in the inset images. TEM micrographs of (c) Fe^0 and (d) Fe_3O_4 nanoparticles with particle size distribution analysis in the inset images.

Foamability and Foam stability

Figs. 4.11 (a) and (b) depict the foamability (MFV) and Figs. 4.11 (c) and (d) reveal the foam stability (RMI 30) of the aqueous APG-Ph surfactant solutions with a varying concentration of Fe^0 and Fe_3O_4 nanoparticles, respectively. The MFV and RMI 30 values are observed to increase with the concentration of surfactant, but the surfactant solution alone shows relatively poor foamability and foam stability even at the highest concentration of 0.1 vol%. With the addition of Fe_3O_4 or Fe^0 nanoparticles, MFV and RMI 30 increase significantly. Fe^0 affects more profoundly than Fe_3O_4. For both the additives, the highest MFV and RMI 30 values are found to occur at the concentration of 3.5 mg/l, along with 0.1% of APG-Ph. Fe^0 produces highest foamability and foam stability of 108.3 mL and 110.4 mL, respectively, whereas Fe_3O_4 particles produce the highest MFV value of 99.4 mL and highest RMI 30 value of 87.5 mL.

At 0.1 vol% concentration of surfactant, for Fe^0 and Fe_3O_4, the foamability increases by 52 and 48%, respectively, compared to that of the surfactant solution alone. Similarly, the foam stability is enhanced by 54% and 42% due to the addition of Fe^0 and Fe_3O_4, respectively. With further increase of particle loading above concentration 3.5 mg/l, the MFV and RMI 30 values are observed to decrease for both the materials. These indicate that the nature and concentration of nanoparticles have significant effects on foamability and foam stability. The results are in concurrence with the existing literature. Significant decrease in foam volume of an aqueous solution of surfactant di-decyl dimethyl ammonium bromide at a high concentration of silica nanoparticle (> 2 wt%) has been reported by (Binks et al., 2008). This reduction in foamability could be explained in terms of the loss of surfactant molecules from the solution as it gets adsorbed on the particle surface.

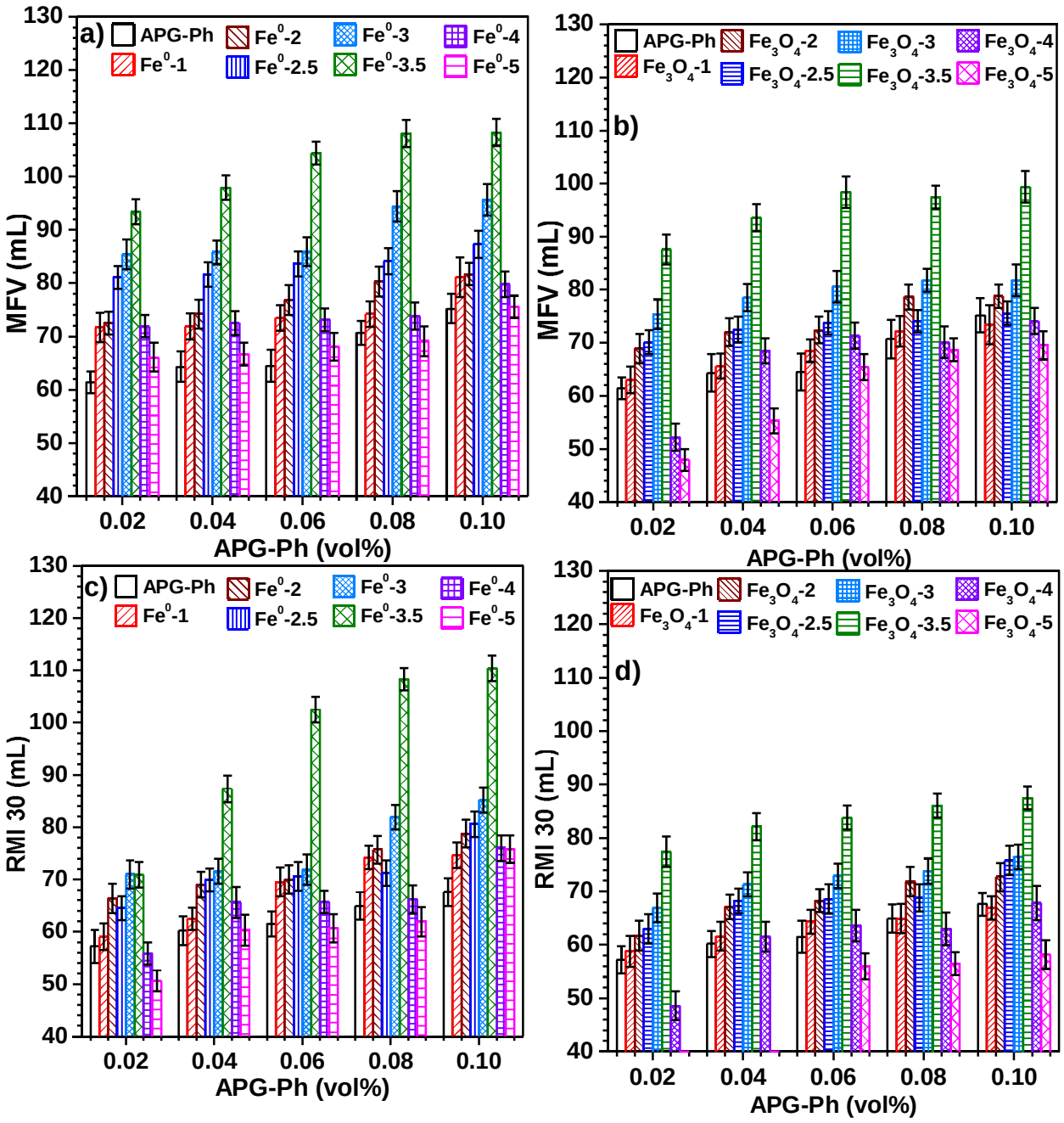

Fig. 4.11 Comparison of (a) and (b) foamability (MFV) and (c) and (d) foam stability (RMI 30) for different concentration aqueous APG-Ph solutions (vol %) and APG-Ph solutions with different concentration of Fe^0 and Fe_3O_4 nanoparticles, respectively. The error bars show the statistical variability of experimental results.

Surface Tension (σ)

Fig. 4.12 shows the variation of surface tension (σ) for aqueous APG-Ph solutions with different surfactant concentrations (vol%) and with different Fe_3O_4 and Fe^0 nanoparticles (3.5, 4, and 5 mg/l) concentrations. Here, the surface tension is used to understand and predict the adsorption behavior of the nanoparticles on the surfactant as it greatly influences the foamability and foam stability (Yazhgur et al., 2013a). As a general trend, a decrease in surface tension is observed with an increase in surfactant concentration. With the addition of Fe^0 and Fe_3O_4 nanoparticles in the surfactant solution, a more significant reduction occurs. The surface tension of pure 0.1 vol% APG-Ph solution is 50.75 mN/m, whereas, it reduces to 9.51 and 19.45 mN/m due to the addition of 3.5 mg/l Fe^0 and Fe_3O_4 powders, respectively. However, a further increase in the concentration of iron and iron oxide nanoparticle in dispersion leads to an increase in surface tension. For 0.1 vol% APG-Ph solution and at particle concentrations of 5 mg/l, the surface tension is observed to be 45.86 and 33.68 mN/m in case of Fe^0 and Fe_3O_4, respectively.

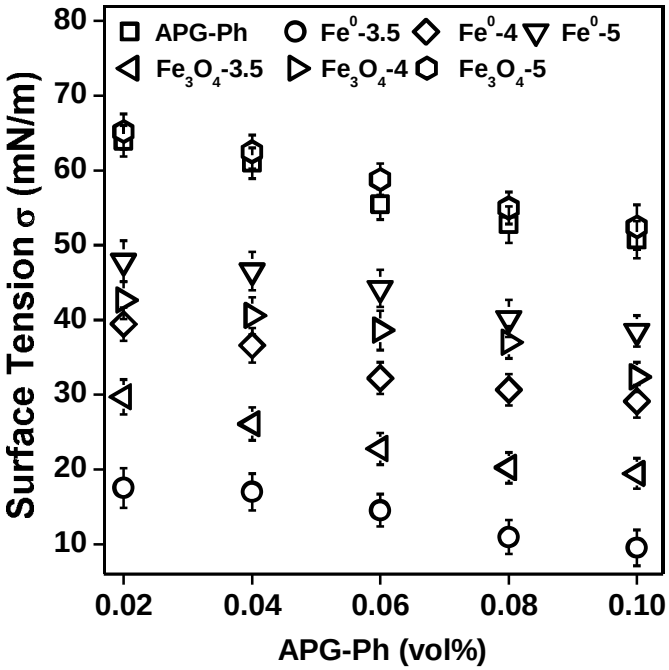

Fig. 4.12 Variation of surface tension for different concentrations of APG-Ph solutions (vol %) and APG-Ph solutions with different concentration of Fe^0 and Fe_3O_4 nanoparticles (3.5, 4 and 5 mg/l)

Zeta Potential (ζ)

Dispersions prepared with Fe^0 and Fe_3O_4 nanoparticles, along with varying concentrations of surfactant, show negative ζ potential, which indicates negative surface charge of the dispersion. The increasing ζ potential with an increase in surfactant concentration towards less negative/more positive value indicates the lower surface charge and higher electrostatic repulsion between the particles. This, in turn, results in reduced aggregation or enhanced stability of the nanoparticles in dispersion (Gumustas et al., 2017; Sharma et al., 2014; Skoglund et al., 2013). The Fe^0 dispersion with 0.1 vol% APG-Ph resulted in highest ζ potential for both the dispersions carrying Fe^0 and Fe_3O_4 nanoparticles (Fig. 4.13), indicating the highest stability.

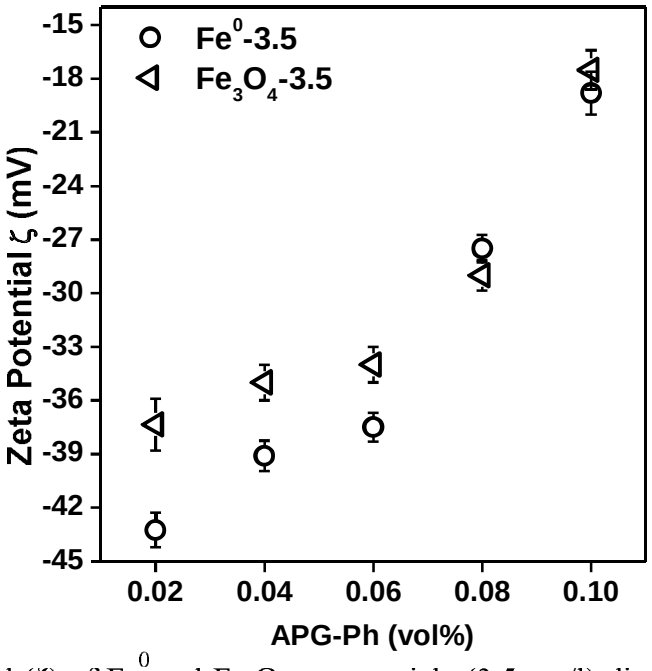

Fig. 4.13 Zeta potential (ζ) of Fe^0 and Fe_3O_4 nanoparticle (3.5 mg/l) dispersions with surfactant concentration. The error bars show the statistical variability of experimental results.

Viscosity (μ)

The viscosity of the Fe^0 and Fe_3O_4 dispersions in deionized water is found to be 2.69 mPa.s and 2.63 mPa.s, respectively (Table 4.2). The viscosity of both the surfactant solution and nanoparticle-surfactant dispersion increases as surfactant concentration increased. The viscosity of 0.1 vol% APG-Ph surfactant solution is found to be 3.85 mPa.s. The maximum viscosity values are observed to be 7.81 and 8.82 mPa.s, for Fe^0 and Fe_3O_4 dispersion, respectively along with 0.1 vol% APG-Ph.

Table 4.2: Viscosity of APG-Ph solution, Fe^0 and Fe_3O_4 (3.5 mg/l) nanodispersion prepared with varying concentrations of APG-Ph shown along with its statistical variation.

APG-Ph (vol %)	Viscosity μ (mPa.s)		
	Only APG-Ph	Fe^0 (3.5 mg/l) + APG-Ph	Fe_3O_4 (3.5 mg/l) + APG-Ph
0	0	2.7 ± 0.30	2.6 ± 0.12
0.02	1.3 ± 0.25	3.4 ± 0.27	4.5 ± 0.20
0.04	1.9 ± 0.15	4.4 ± 0.16	5.4 ± 0.15
0.06	2.5 ± 0.31	5.5 ± 0.15	6.6 ± 0.11
0.08	2.9 ±0.35	6.5 ± 0.28	7.8 ± 0.52
0.1	3.9 ± 0.46	7.8 ± 0.62	8.8 ± 0.12

Remediation of diesel-contaminated soils

Fig. 4.14 demonstrates the comparative study of efficiency (%) of diesel removal from (a) desert soil, (c) coastal soil, & (e) clay soil after 3 h treatment with different concentrations of APG-Ph solution, APG-Ph foam, and APG-Ph - Fe_3O_4 & APG-Ph - Fe^0 dispersions (3.5 mg/l). The APG-Ph-Fe^0 dispersions show higher removal efficiency than that of the APG-Ph-Fe_3O_4 dispersion, APG-Ph solution, and APG-Ph foam. For 0.1 vol% APG-Ph solution, the maximum diesel removal efficiency from the desert soil, coastal soil, and clay soil are observed to be 49.6,

46.3, and 18.6 %, respectively. On the other hand, 0.1 vol% APG-Ph foam results in 56.2, 59.1 and 20.8 % diesel removal efficiency from the desert soil, coastal and clay soil, respectively. The dispersion of 3.5 mg/l of Fe_3O_4 in 0.1 vol% APG-Ph shows 49.0, 44.1, and 22.5 % maximum diesel removal from desert soil, coastal soil, and clay soil, respectively. Whereas, the 3.5 mg/l of Fe^0 dispersion in 0.1 vol% APG-Ph demonstrates 72.5, 60.3 and 42.5% maximum diesel removal from desert soil, coastal soil and clay soil, respectively.

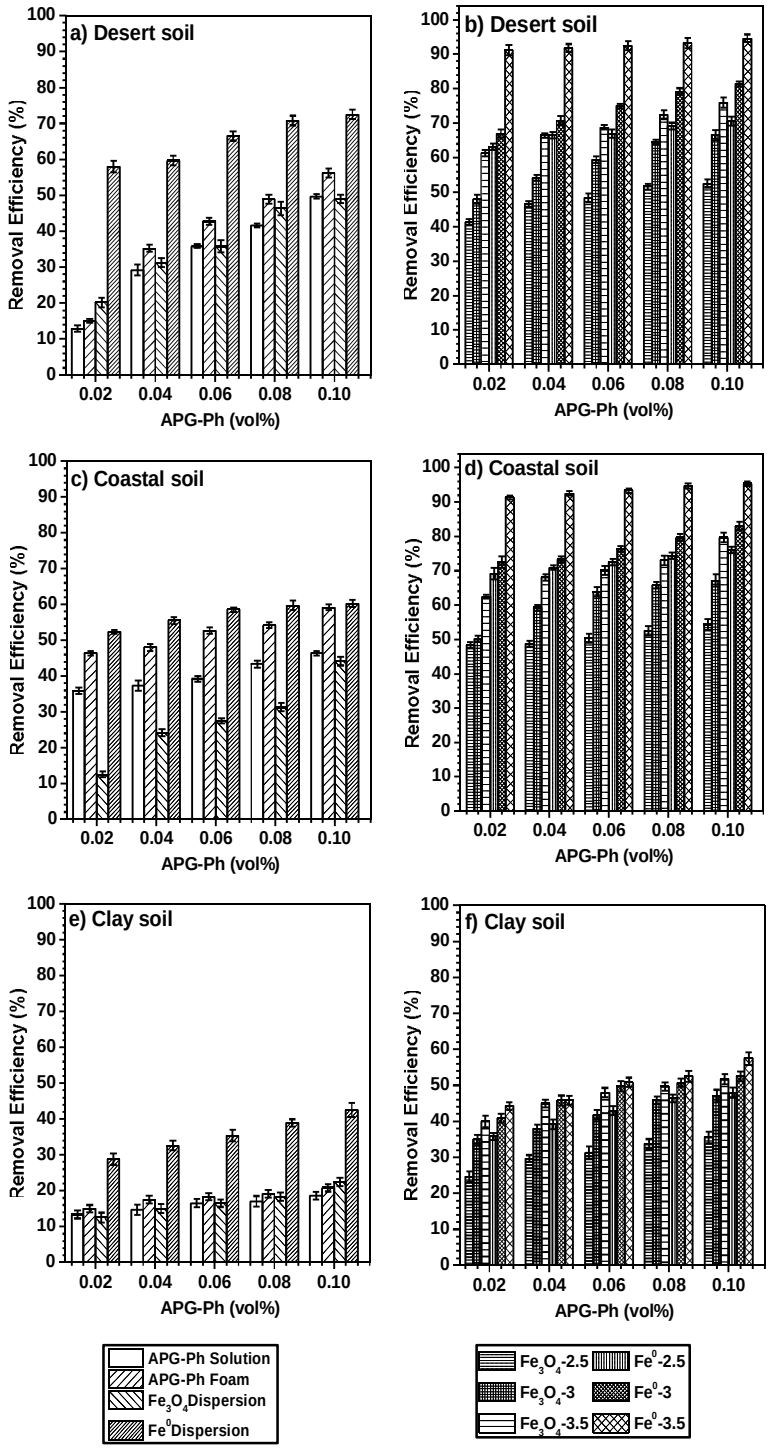

Fig. 4.14 Comparison of diesel removal efficiency (%) for (a) desert soil, (c) coastal soil, & (e) clay soil after 3 h treatment with different concentrations of APG-Ph solution, APG-Ph foam, and APG-Ph - Fe_3O_4 & APG-Ph - Fe^0 dispersions (3.5 mg/l) and (b) desert soil, (d) coastal soil, and (f) clay soil after 3 h treatment with APG-Ph foam stabilized by Fe_3O_4 and Fe^0 nanoparticle (2.5, 3 & 3.5 mg/l). The error bars show the statistical variability of experimental results.

Table 4.3: Comparison of the properties of the natural soils (refers to soils without any contamination), contaminated soils and soils after the remediation process with 0.1 vol % APG-Ph foam stabilized by 3.5 mg/l Fe^0 and Fe_3O_4 nanoparticles shown along with statistical variation.

Elements (wt %)/ Properties	Desert Soil				Coastal Soil				Clay Soil			
	NS	DSNL	After Remediation with NP stabilized foam		NS	DSNL	After Remediation with NP stabilized foam		NS	DSNL	After Remediation with NP stabilized foam	
			Fe^0NP	Fe_3O_4NP			Fe^0NP	Fe_3O_4NP			Fe^0NP	Fe_3O_4NP
C	14.1±0.5	33.3±0.62	2.3±0.69	7.2 ±1.2	15.5	49.3±5.84	4.4±2.72	14±3.5	12.6±2.5	29.9±2.33	14.2±4.69	10.9±2.3
O	54.9±3.5	36.5±5.5	51.9±0.48	41.9 ±3.5	52.2	27±4.67	53.6±6.03	53±5.5	51.5±6.5	40.3±3.16	41.7±1.46	43.9±4.6
Mg	0.8±0.2	0.4 ±0.01	0.4±0.18	0.4 ±0.1	-	-	-	-	1.3±3.9	1±0.2	0.9±0.11	0.89±0.5
Si	24±1.2	12.7±0.62	21±1.24	22.3±2.2	25	16.8±2.18	21.3±5.37	21.4±2.3	15.1±4.5	9.8±0.56	11.6±0.62	14.07±2.9
K	0.5±0.05	0.6±0.17	0.7±0.06	0.4±0.2	0.7	0.4±0.15	0.5±0.39	0.3±0.06	1.1±3.6	1.2±0.15	1.2±0.05	0.7±0.3
Ca	0.2±0.1	1.6±0.13	0.4±0.12	0.6 ±0.35	0.3	0.4±0.12	0.8±0.25	0.4±0.2	0.8±1.2	0.6±0.0.8	0.5±0.07	0.4±0.08
Fe	1.5±0.5	1.2±0.69	2.4±0.01	0.9±0.4	1.4	1.5±0.2	2.15±0.72	1.9±0.09	7.8±3.2	6.3±0.58	5.7±0.35	4±1.02
Pb	-	2.9±0.30	0.3±0.23	0.6±0.37	-	0.08±0.01	0.1±0.03	0.07±0.01	-	0.1±0.02	0.12±0.03	0.06±0.01
Al	3.8±0.95	3.9 ±1.7	4.2±1.02	8.4±2.2	4.4	4.8±0.37	10.7±2.52	5.6±6.6	7.4±3.2	6.4±0.71	6.4±0.35	6.3±2.1
As	-	2.4 ±0.2	1.06±0.12	0.08±0.02	-	0.7±0.07	0.6±0.18	0.4±0.2	-	0.8±0.19	0.6±0.19	0.6±0.3
pH	8.2±0.07	8.5±0.09	8.2±3.06	8.19±0.06	8.4±1.2	8.5±0.24	8.3±0.08	8.4±0.06	7.5±0.42	7.9±0.02	7.4±0.13	7.9±0.5
Conductivity (*10^{-4} S/m)	233 ± 5.6	239 ± 4.5	240.3±5	242.5±4.2	176±2.8	178±2.56	181.6±3.6	185±4.8	831±5.65	845±5.35	875±5.35	876±6.35

NS: Natural Soil; **DSNL**: Diesel contaminated natural soil; **NP**: Nano particles

Figs. 4.14 displays diesel removal efficiency (%) from (b) desert soil, (d) coastal soil, and (f) clay soil after 3 h treatment with different concentrations of APG-Ph foam stabilized by Fe_3O_4 and Fe^0 nanoparticles (2.5, 3 & 3.5 mg/l). The removal efficiency gradually increases with the rise in the concentration of APG-Ph (Figs. 4.14 a, c, and e), but significant increases are noticed with the addition of nanoparticles. The foam stabilized by Fe_3O_4 (3.5 mg/l) shows the maximum removal efficiency of 76.0% at the surfactant concentration (0.1 vol%) for desert soil. The coastal soil and clay soil, treated with the same foam, show 79.6 and 51.6% efficiency, respectively. The maximum diesel removal efficiency of 95.3 % is achieved by 3.5 mg/l Fe^0 stabilized APG-Ph foam (0.1 vol%) applied on coastal soil. The desert soil and clay soil show maximum of 94.6 and 57.5 % diesel oil removal, respectively, when treated with the same foam. The elemental composition of natural soil (refers to soil without any contamination), contaminated soil, and soil after the remediation process are measured using EDX and shown in Fig. 3.1. EDX analysis reveals that the carbon content of the soils increases with the addition of diesel, as expected because the major constituents of diesel are hydrocarbons. The carbon content of contaminated coastal, desert and clay soils is 49.3, 33.3 and 29.9 wt %, respectively (Table 4.3). After treatment with 3.5 mg/l Fe^0 stabilized 0.1 vol% APG-Ph foam, diesel left in the soil is reflected well in the carbon content measurement by the EDX; 4.6, 2.3, and 14.2 wt. % for coastal, desert and clay soil, respectively. Also, the elemental analysis shows reduction of certain heavy metals (Ca, Pb, As) in the contaminated soil after treatment process (Table 4.3). Although no particular trend could be found in the change of pH and conductivity in the soils before and after treatment.

The diesel removal efficiency increases rapidly as the foam stability increases. The results are found to be comparable with that reported previously in the literature. (Khalladi et al., 2009)

achieve 93 % diesel removal efficiency from soil comprising 94 % silt by using SDS solution flushing. The major observation from their study is that the elimination rate of diesel from soil depends on the time duration of the flushing process. (Couto et al., 2009) report a 99 % removal efficiency of diesel oil from the contaminated sandy soil by treating with surfactant foam. (Li et al., 2015) report a 50 % removal efficiency by washing the crude oil contaminated clay soil with nonionic surfactant Tween 20.

Kinetics

Variation of residual diesel concentration (C_t) in different soils with treatment time (min) for Fe^0 (3.5 mg/l) and Fe_3O_4 (3.5 mg/l) nanoparticle stabilized APG-Ph (0.1 vol%) foam is illustrated in Fig. 4.15. The results indicate that the amount of diesel removal depends on the time of treatment, the stability of the foam, and properties of the soil. The foam stabilized by Fe^0 takes 3h for removing 94.6 and 95.3 % of diesel from desert soil (DS) and coastal soil (CS), respectively. The foam stabilized by Fe_3O_4 achieves only 76.0 and 79.6 % removal efficiency from the desert and coastal soil, respectively, after 3h of treatment. Whereas, in the same time period, both Fe^0 and Fe_3O_4 nanoparticle stabilized APG-Ph (0.1 vol%) foam could remove only 57.5 and 51.6 % of diesel, respectively, from the clay soil (CLS). This indicates the formation of a relatively stronger interaction bond between the contaminant diesel oil on the coastal soil or desert soil and the Fe^0 and Fe_3O_4 stabilized foam during the flushing process. Soil structure, especially high porosity in clay soil might have influenced the slow removal of diesel contaminant.

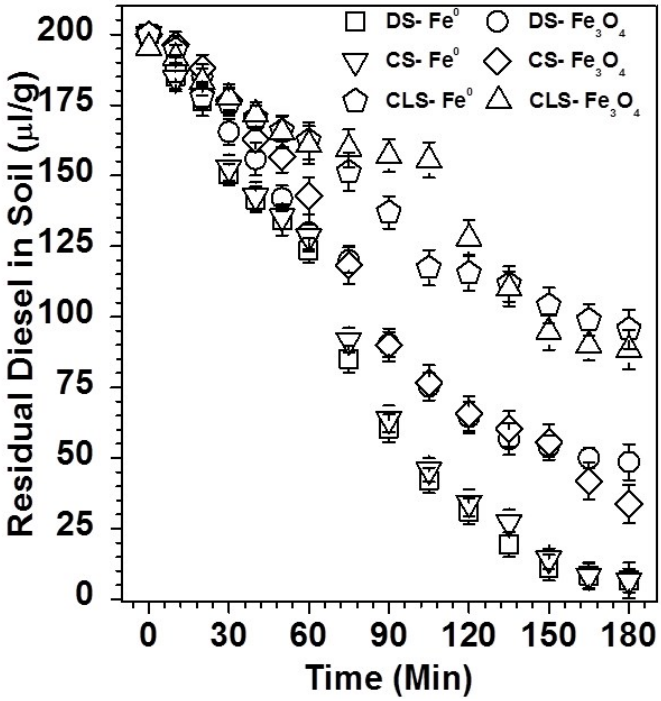

Fig. 4.15 Variation of diesel concentration (C_t) remaining in soil with treatment time (a) for Fe^0 and Fe_3O_4 nanoparticle (3.5 mg/l) stabilized APG-Ph (0.1 vol %) foams for different soils.
Note: DS→ desert soil, CS → coastal soil, & CLS → clay soil

The experimental results show a reasonably good fit with the first order Fig. 4.16 (a) rate equation than the second-order Fig. 4.16 (b). As it is clear from the inset plot of Fig. 4.16 (a), clay soil shows two distinct linear fitting regions in the first-order kinetic plot. The first region, completed after around 110 minutes both for Fe^0 and Fe_3O_4 stabilized foam, indicates a slower rate of diesel removal and corresponds to stronger binding of the contaminant diesel with soil and also a restrictive diffusion of foam in the clay's pores (Silcox et al., 1995). The first-order rate constant for Fe^0 nanoparticle is obtained as 0.0111, 0.0118, 0.0021 µl g^{-1} min^{-1} for desert soil, coastal soil, and clay soil, respectively. Similarly, the rate constant obtained for Fe_3O_4 nanoparticle is 0.0041, 0.0045, and 0.0028 µl g^{-1} min^{-1} for desert soil, coastal soil, and clay soil, respectively as shown in Fig. 4.16 (b). In a similar study (Khalladi et al., 2009) report the diesel removal by SDS solution as a first-order kinetic process.

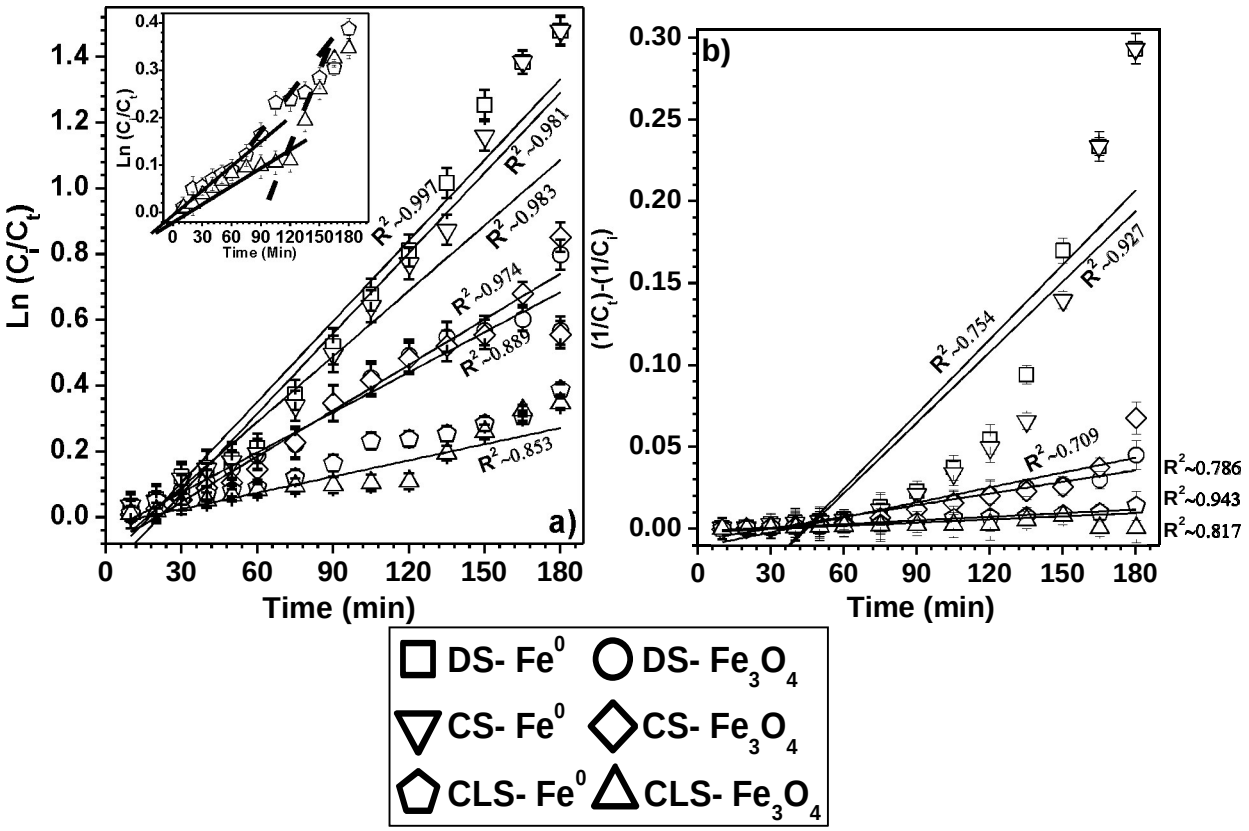

Fig. 4.16 (a) The first order rate kinetics [ln (C_i/C_t) vs time] data fitting for oil removal from various soils. The inset figure shows the presence of two distinct regions of linear fit for the clay soil. (b) The second order rate kinetics [$(1/C_t)$ -$(1/C_i)$ vs time] data fitting for oil removal from various soils, as comparison. The error bars show the statistical variability of experimental results.
Note: DS→ desert soil, CS → coastal soil, & CLS → clay soil

Residual iron concentration in soil

Fig. 4.17 shows the variation in residual iron concentration left in different soils following the treatment with different concentrations of Fe^0 and Fe_3O_4 stabilized 0.1 vol% APG-Ph aqueous foams for 3 h. In general, the amount of nanoparticles adhered in soil is found to increase with the concentration of nanoparticles in the injected foam. The maximum amount of iron retention is observed in the clay soil (0.7254 mg/l) treated with Fe^0 nanoparticle (3.5 mg/l) stabilized foam. On the other hand, desert soil and coastal soil retain 0.636 and 0.6871 mg/l of iron, respectively after treatment with the same foam. After being treated with Fe_3O_4 nanoparticle (3.5 mg/l) stabilized foam, the maximum retention of iron is found to be 0.492, 0.625, and 0.689 mg/l in the

desert soil, coastal soil, and clay soil, respectively. As the clay content in the desert and coastal soil is negligible, the mobility of iron nanoparticles through the soil is high, and hence, lower (~14% of the total) retention of iron is observed. It could have been possible to achieve lesser retention of iron by avoiding the aggregation of nanoparticle on the soil surface. Nanoparticles aggregated on the soil would block the available sites due to electrostatic repulsion. Further, the blocking would result in less availability of iron particles for the removal of the contaminant from the soil (Zhang et al., 2017).

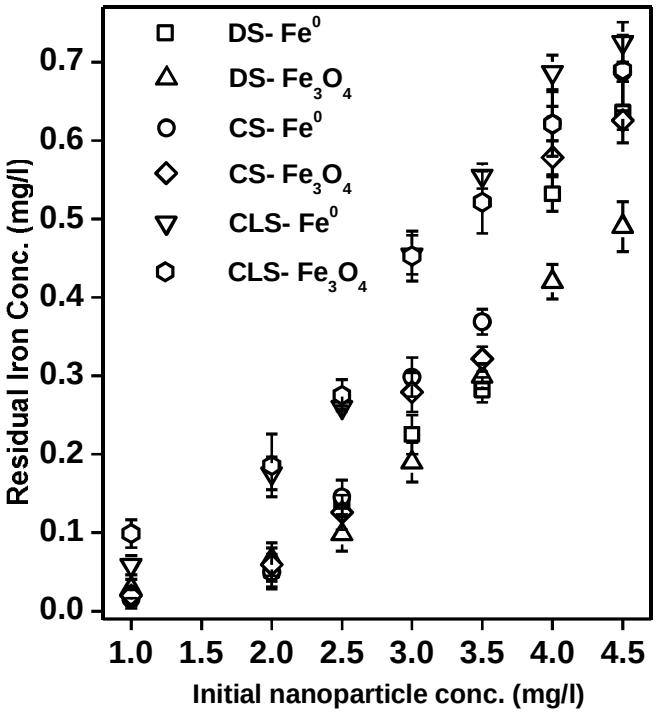

Fig. 4.17 variation of residual iron concentration in different soils after treatment with different concentration of Fe^0 and Fe_3O_4 stabilized (0.1 vol %) APG-Ph foams. Note: DS→ desert soil, CS → coastal soil, & CLS → clay soil

Residual diesel contaminant in soil

Fig. 4.18 (a), (b), and (c) show the TGA thermographs of diesel-contaminated desert soil, coastal soil, clay soil, and soils after treatment with Fe^0 and Fe_3O_4 nanoparticle (3.5 mg/l) stabilized (0.1 vol%) APG-Ph foam. Initially, the gradual decrease in weight of soil contaminated with diesel on day 1 (profile 1) and day 7 (profile 2) indicate the progressive volatilization of diesel from the soil, and no significant weight loss is observed above 250°C. The clay soil shows the highest weight loss of ~ 30% due to the presence of organics and microbes on the surface. In the case of Fe^0 treated (profile 3) desert soil and coastal soil, the diesel remaining in the soil is effectively low, and hence the least weight loss is found in the TGA plot. Similarly, the soils treated with Fe_3O_4 stabilized foam (profile 4) have an intermittent weight loss, accounting for 76% of diesel removal efficiency achieved. Clearly, the amount of diesel remaining in clay soil treated with Fe^0 stabilized foam is lower compared to that of the Fe_3O_4 stabilized foam treated clay soil. Also, the APG-Ph foam (profile 5) could remove less diesel oil from the soils as compared to the Fe^0, or Fe_3O_4 nanoparticle stabilized foams. Hence, the weight loss of diesel is higher.

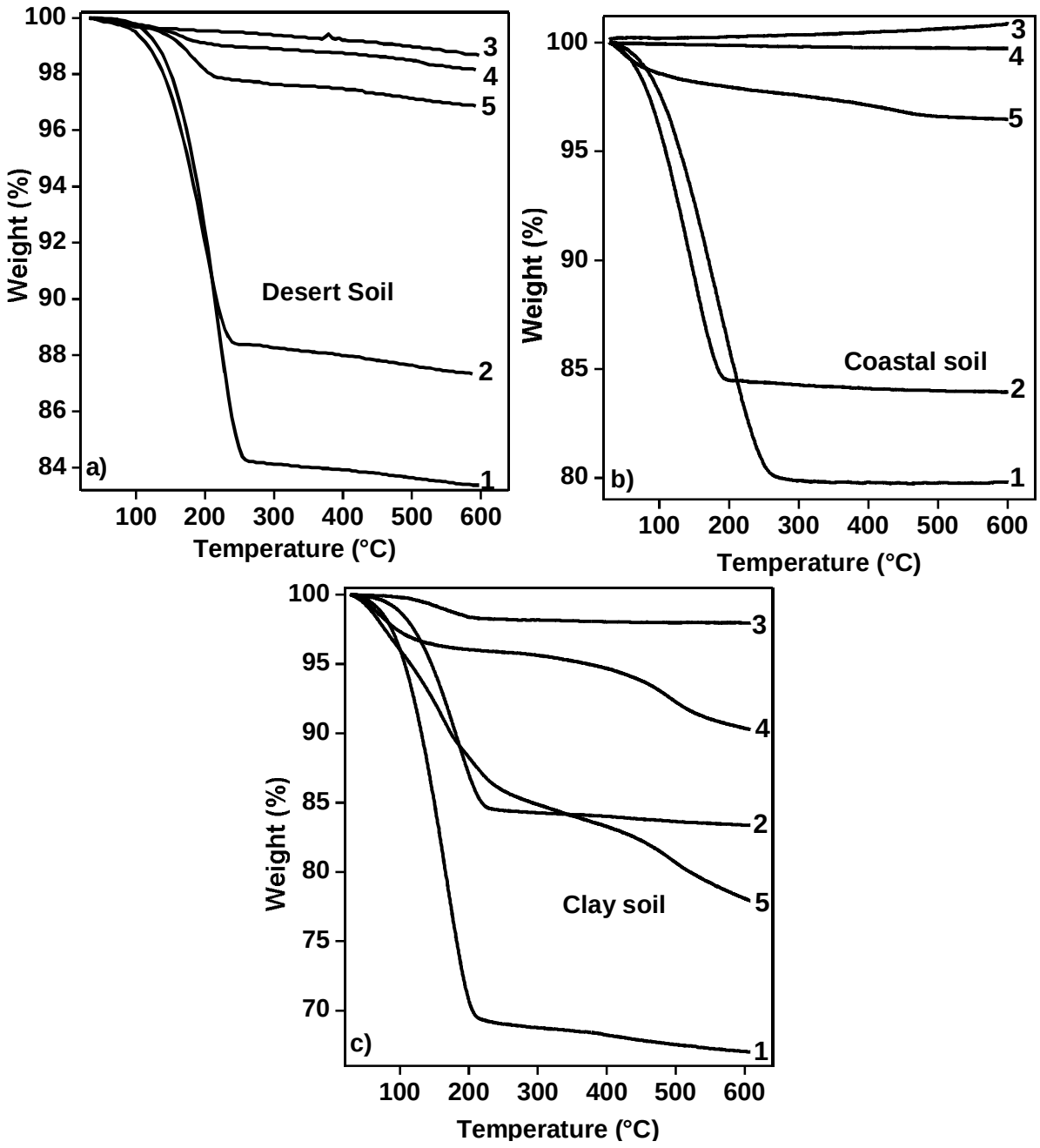

Fig. 4.18 TGA scans showing variation of the amount of diesel contaminants left in (a) Desert soil, (b) Coastal soil, and (c) Clay soil; profiles 1 & 2- data obtained from soil after one day of contamination and after seven days of contamination before treatment, respectively, profiles 3 & 4– from soil after treatment with Fe0 and Fe3O4 nanoparticle (3.5 mg/l) stabilized (0.1 vol %) APG-Ph foams, respectively, and profile 5- from soil treated with only (0.1 vol %) APG-Ph foam.

4.1.4 Numerical optimization of APG-Ph foam stabilized with Fe^0 nanoparticle in Remediation of Diesel Contaminated Soils Using RSM

Table 4.4 shows the foam properties of the APG-Ph foam stabilized with Fe^0 at various concentrations, and the same is utilized in the treatment of contaminated soils. The foamability and foam stability are depicted as MFV and RMI 30 in the present work. As it can be seen that, with an increase in the concentration of APG-Ph the foamability and foam stability increases. Addition of Fe^0 in the surfactant solution a significant increase in the MFV and RMI 30 is observed. The highest MFV and RMI 30 values are achieved at 3.5 mg/l of Fe^0 in 0.1 vol% APG-Ph. The results are consistent with the results reported in literature. (Wang et al., 2015c) evaluate the foam properties of the surfactant and represent the foamability and foam stability. The foam volume increases with an increase in the surfactant concentration until a threshold concentration of 3.5 mg/l. With further addition of Fe^0 nanoparticle above the concentration of 3.5 mg/l the MFV and RMI 30 values are seen to decrease, indicating that the concentration of nanoparticles has significant effects on foamability and foam stability.

Table 4.4: Foamability (MFV) and foam stability (RMI 30) for different concentrations of aqueous APG-Ph solution (vol%) and APG-Ph with different concentration of Fe^0.

APG-Ph Conc. (vol%)	Fe^0 Conc. (mg/l)	MFV (mL)	RMI 30 (mL)
0.02	2.5	81.1	64.5
0.04		81.6	69.9
0.06		83.6	70.6
0.08		84.1	71.2
0.1		87.3	80.6
0.02	3	85.4	71
0.04		85.8	71.6
0.06		85.9	71.9
0.08		94.4	81.9
0.1		95.6	85.2
0.02	3.5	93.4	70.9
0.04		97.9	87.3
0.06		104.4	102.5
0.08		108.1	108.3
0.1		108.3	110.4

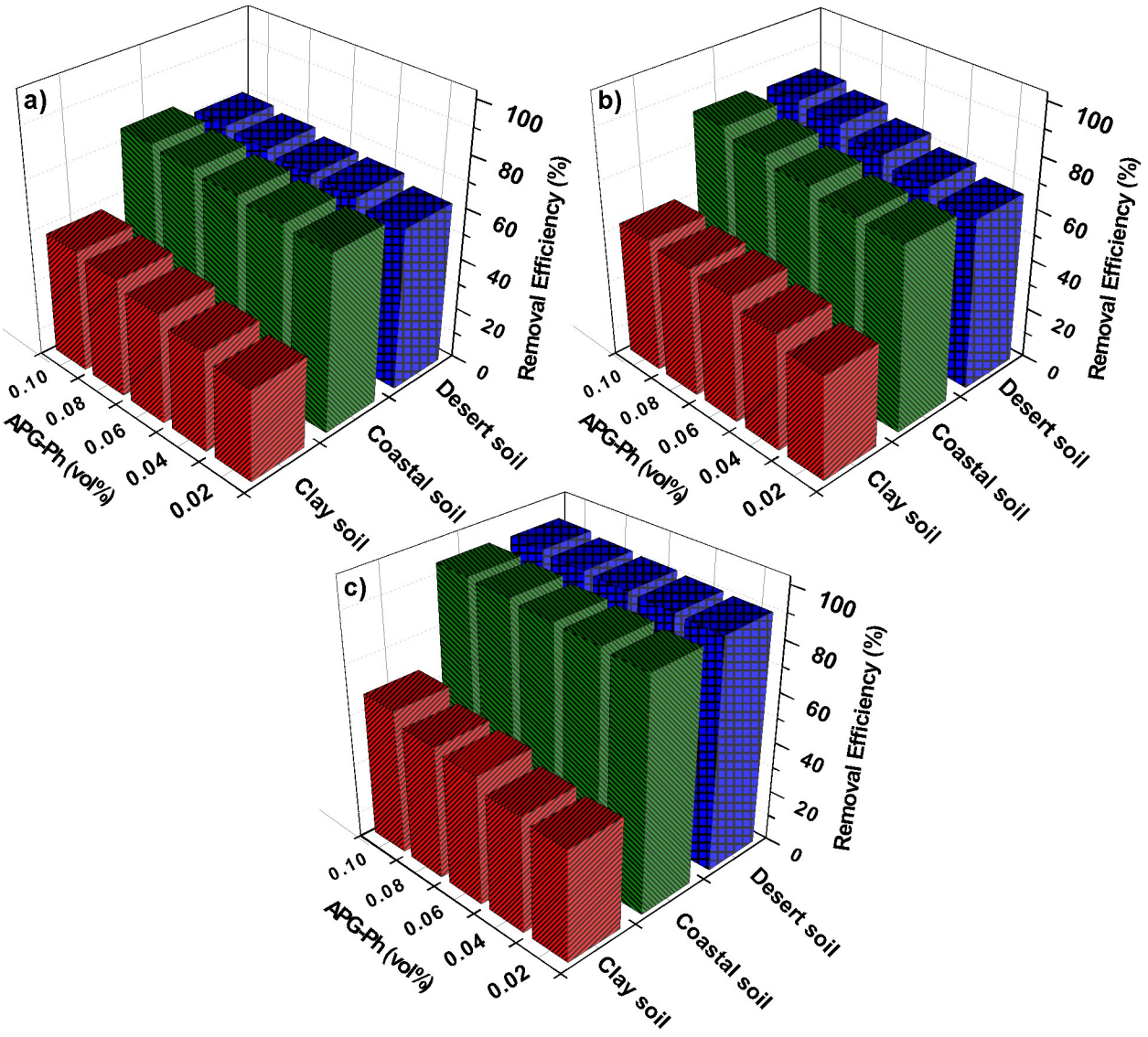

Fig. 4.19 Comparison of diesel removal efficiency (%) from desert soil, coastal soil, clay soil after treatment with different concentrations of APG-Ph foam, stabilized by Fe^0 at various concentrations (a) 2.5 mg/l, (b) 3 mg/l and (c) 3.5 mg/l.

It is clearly observed that the foam stabilized with Fe^0 shows the highest MFV and RMI values and maximum diesel removal efficiency from the soil. Fig. 4.19 shows the 3D representation of diesel removal efficiency from three different soils (Coastal, desert, and clay soil) at different concentrations of APG-Ph foam stabilized by (a) 2.5 mg/l (b) 3 mg/l and (c) 3.5 mg/l of Fe^0. The diesel oil removal efficiency increases as the concentration of APG-Ph

increases. Also, the increase in removal efficiency is noted with an increase in the concentration of Fe^0. The foam stabilized by 3.5 mg/l of Fe^0 shows maximum removal efficiency for all three soils. By using the foam stabilized by 0.1 vol% APG-Ph and 3.5 mg/l Fe^0, the maximum removal efficiency values achieve for the coastal and desert soils are 95.3 and 94.6%, respectively, whereas only 57.5% removal efficiency is observed in case of the clay soil.

Effect of process variables on removal efficiency

Table 4.5 shows the results of targeted response (soil removal efficiency) from three different soils with respect to the treatment of APG-Ph foam stabilized by Fe^0 obtained using full factorial BBD. The soil removal efficiency is established based on the interactions of the independent variables (concentration of APG-Ph and Fe^0). Both of these independent variables significantly influence the diesel removal efficiency from contaminated soil. The statistical significance of the quadratic model id evaluated using ANOVA (Table 4.6). The significance of the model is tested using P-values and the R^2 values provide the goodness of the fit (Dahiru, 2008). The final equation is framed using the coefficient values of the response targeted. After neglecting insignificant terms, the p-values obtained for the model is significantly low ($p< 0.0001$ & $p< 0.05$) which indicates the importance of the model. Also, the high R^2 values indicate the high statistical connotation of the predicted model (Balakrishnan and Rajeswari, 2018). The R^2 values obtained for the response removal efficiency from desert coastal and clay soils are 0.9828, 0.9854 and 0.9264, respectively.

Table 4.5: Experimental range of independent variables used in the full factorial of BBD design matrix with the response (removal efficiency) for desert coastal and clay soil.

Run. No	Independent variables		Response (Y_1: Removal Efficiency (%) from desert soil)		Response (Y_2: Removal Efficiency (%) from coastal soil)		Response (Y_3: Removal Efficiency (%) from clay soil)	
	APG-Ph Conc. :X_1	Fe^0 Conc:X_2	Expt. Data	RSM Pred	Expt. Data	RSM Pred	Expt. Data	RSM Pred
1.	0.0	3.0	70.7	72.2	76.0	75.3	48.0	45.0
2.	0.1	2.5	67.0	68.4	72.5	73.1	40.8	42.7
3.	0.0	3.0	70.8	73.7	73.2	76.0	45.8	46.9
4.	0.1	3.0	75.0	75.3	76.3	77.1	49.8	49.1
5.	0.1	3.0	79.2	77.0	79.7	78.8	50.7	51.5
6.	0.1	3.0	81.3	78.9	83.0	81.0	52.5	54.3
7.	0.0	3.5	91.2	89.9	91.3	91.3	44.2	44.8
8.	0.0	3.5	91.8	91.2	92.5	91.9	45.8	47.2
9.	0.1	3.5	92.5	92.6	93.3	92.9	50.8	49.9
10.	0.0	2.5	63.2	62.9	69.2	69.4	35.8	37.8
11.	0.1	3.5	93.3	94.1	94.7	94.5	52.5	52.9
12.	0.1	3.5	94.7	95.8	95.3	96.6	57.5	56.2
13.	0.0	2.5	66.5	64.6	70.8	70.1	39.2	39.1
14.	0.1	2.5	67.0	66.4	72.5	71.4	43.3	40.7
15.	0.1	2.5	69.2	70.5	74.3	75.4	46.3	44.9

Note: **Expt**- Experimental, **Pred**- Predicted,

Table 4.6: ANOVA for the responses: diesel oil removal efficiency from desert, coastal and clay soil.

Source	(Y_1: Removal Efficiency (%) from desert soil)					(Y_2: Removal Efficiency (%) from coastal soil)					Y_3: Removal Efficiency (%) from clay soil				
	SS	**df**	**MS**	**F**	**p**	**SS**	**df**	**MS**	**F**	**p**	**SS**	**df**	**MS**	**F**	**p**
Model	1853.7	5	370.7	103	<0.0001	1310.3	5	262.1	121.9	<0.0001	425.1	5	85.0	22.6	<0.0001
X_1	2.3	1	2.3	0.6	0.4	0.1	1	0.1	0.0	0.9	1.2	1	1.2	0.3	0.6
X2	31.5	1	31.5	8.8	0.0	55.2	1	55.2	25.7	0.0	53.0	1	53.0	14.1	0.0
X_1 X_2	0.8	1	0.8	0.2	0.6	0.2	1	0.2	0.1	0.8	5.7	1	5.7	1.5	0.2
X_1^2	0.2	1	0.2	0.0	0.8	2.7	1	2.7	1.3	0.3	1.0	1	1.0	0.3	0.6
X_2^2	59.7	1	59.7	16.6	0.0	83.9	1	83.9	39.0	0.0	47.3	1	47.3	12.6	0.0
Residuals	32.4	9	3.6			19.4	9	2.2			33.8	9	3.8		
F-value probability	<0.001					<0.001					<0.001				
R^2	0.9828					0.9854					0.9264				
Adj. R^2	0.9733					0.9774					0.8854				
Predicted R^2	0.9487					0.9573					0.7360				

Note: **SS**- Sum of Squares **df**- Degree of Freedom, **MS**- Mean Square, **p**- Probability.

The selected independent variables (APG-Ph and Fe^0 concentrations) which affect the targeted response (diesel oil removal efficiency) are envisaged after fitting the model. Based on the multiple linear equations the interaction between the process variable and the response is evaluated by plotting 3D surface plots and contour plot. The 3D plot obtained from RSM helps to correlate the interaction between the independent variables and response. The experimental results are analyzed using multiple linear regressions. The predicted R^2 value of desert, coastal and clay soil are 0.9487, 0.9573 and 0.7360, respectively. The predicted R^2 values matched the adjusted R^2 values of desert, coastal and clay soil. The adjusted R^2 values are 0.9733, 0.9774 and 0.8854 for desert, coastal and clay soil, respectively. The responses Y_1 and Y_2 showed a high R^2 value, whereas, the response Y3 showed a low R^2. This indicates that the developed RSM model is highly reliable for optimizing the diesel removal efficiency from the desert and coastal soil compared to that of clay soil. Also, the optimization depends on the type of soil used. The results are in agreement with the previously reported results in the literature (Gharibzadeh et al., 2018). The model equation for removal efficiency from the desert (Y_1), coastal (Y_2) and clay soil (Y_3) is given below,in terms of coded factors:

$$Y_1(\%) = 141.18 + 125.4\,X_1 - 74.27\,X_2 - 20\,X_1X_2 + 158.73\,X_1^2 + 16.93\,X_2^2 \quad (20)$$

$$Y_2(\%) = 189.39 + 22.42\,X_1 - 98.28\,X_2 - 9.17\,X_1X_2 + 634.92\,X_1^2 + 20.07\,X_2^2 \quad (21)$$

$$Y_3(\%) = 109.93 - 90.04\,X_1 + 96.33\,X_2 + 53.33\,X_1X_2 + 386.91\,X_1^2 - 15.07\,X_2^2 \quad (22)$$

The final equation in terms of actual factors:

$$Y_1(\%) = 141.1778 + 125.3965\,X_1 - 74.2668\,X_2 - 20\,X_1X_2 + 158.7321\,X_1^2 + 16.933\,X_2^2 \quad (23)$$

$$Y_2(\%) = 189.3944 + 22.4204\,X_1 - 98.2833\,X_2 - 9.1666\,X_1X_2 + 634.9202\,X_1^2 + 20.0666\,X_2^2 \quad (24)$$

$$Y_3(\%) = 109.9333 - 90.0398\,X_1 + 96.3333\,X_2 + 53.3333\,X_1X_2 + 386.9053\,X_1^2 - 15.0667\,X_2^2 \quad (25)$$

Fig. 4.20 (a), (b) and (c) shows experimental values pertaining to the removal efficiency from different soils and the predicted values by the developed model equation. The experimental data points are consistent with the predicted values. The high regression coefficient values show that the fitted model is accurate to predict the targeted response using BBD. The difference between the observed value and predicted value of the response is denoted by the term 'residual' and its analysis provides the adequacy of the developed model. Fig. 4.20 (d), (e) and (f) show the plot of studentized residuals vs. predicted values. The residuals are scattered at random in the range of (-3 and 3). A random scatter explains the non-violation of equality of variance (Long et al., 2013).

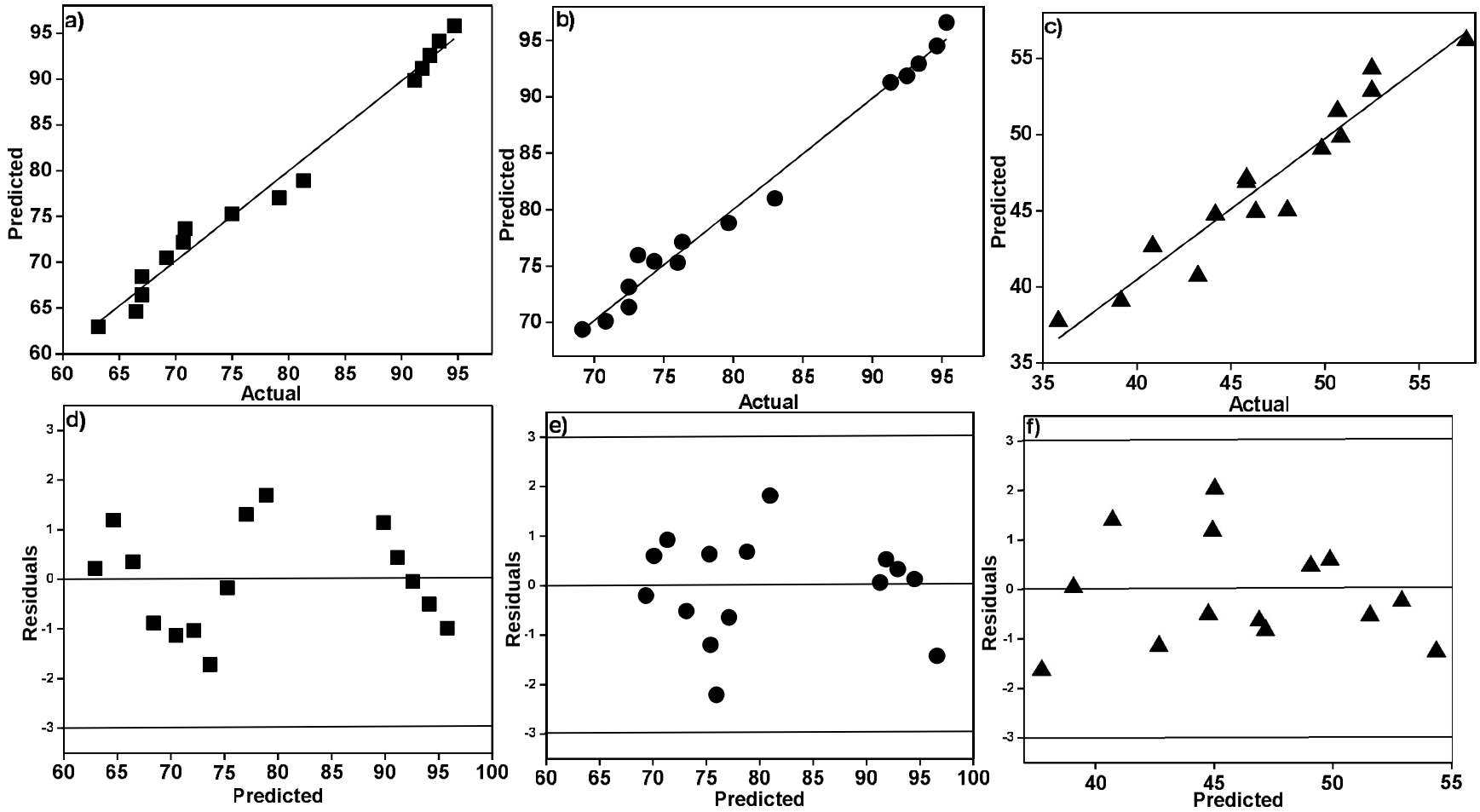

Fig. 4.20 Plot of experimental values of removal efficiency (a) desert soil (b) coastal soil and (c) clay soil compared to the predicted values by the developed model equation using RSM. (d) desert soil (e) coastal soil and (f) clay soil studentized residual Vs. predicted values.

Response surface

The 3D response surface plot for the diesel oil removal efficiency from contaminated soils is plotted against the two independent process variables. The surface plot is developed by using the quadratic model equations (Eqs.20-25). Three-dimensional graphs are helpful in understanding the interaction between the process parameters and their influence on the response targeted (Kılıç et al., 2013). Also, these plots provide a significance about the geometric nature of the response plot developed and the coefficients obtained for the model equations (Prakash et al., 2008). Fig. 4.21 (a), (b) and (c) shows the effect of independent variables APG-Ph and Fe^0 concentrations on the diesel oil removal efficiency from the contaminated desert, coastal and clay soils, respectively. It can be observed from the graph that with the increase in the APG-Ph concentration from 0.02 to 0.1 vol% the removal efficiency increases regardless of types of soil. Also, with an increase in Fe^0 concentration from 2-3.5 mg/l the removal efficiency increased rapidly. At 3 mg/l of Fe^0, the maximum diesel removal efficiency is achieved. In the surfactant foam system stabilized by Fe^0, the interaction of nanoparticle with the contaminant tends to oxidize it rapidly (Raychoudhury and Scheytt, 2013). The results are in concurrence with the existing literature. (Chang and Kang, 2009) conducted experiments to study the pyrene removal from contaminated soil using Fe^0. Numerical optimization provides a desirable value for all the input factors and selected response. In RSM, numerical optimization can be performed to obtain optimized output by setting the input factors as the range, maximum, minimum for the selected responses (Mourabet et al., 2017). The results are optimized using the polynomial equation developed using the RSM. In the optimization process, the independent variables APG-Ph and Fe^0 concentrations are selected to be in range and diesel removal efficiency from soil is chosen to be maximized.

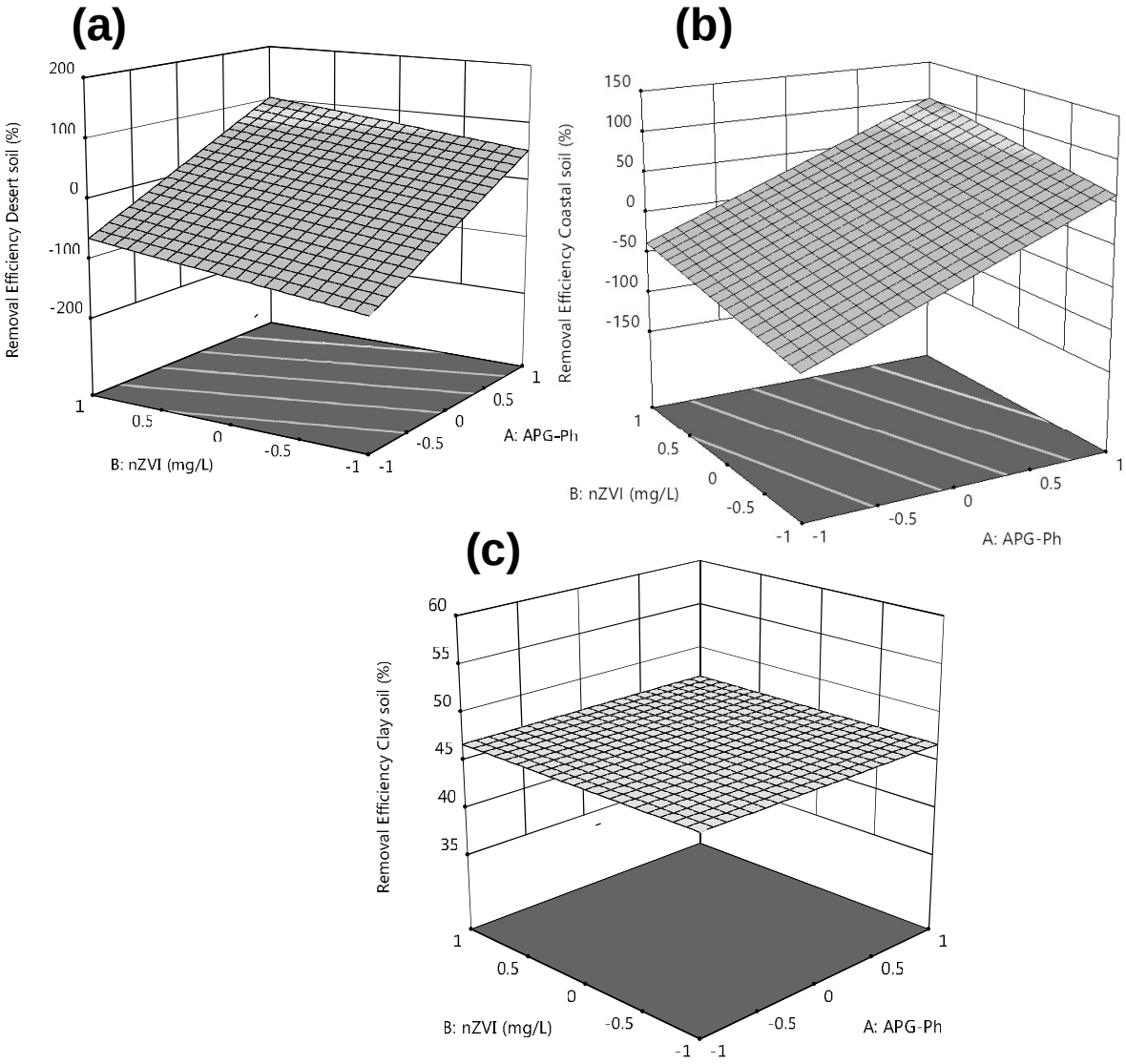

Fig. 4.21 Three dimensional Response surface plot developed by RSM showing diesel removal efficiency from (a) desert soil (b) coastal soil and (c) clay soil as a function of independent variables APG-Ph (X1) & Fe^0 (X2) concentration.

In the current study, the input variables are selected to be in range and the response is desired to be maximized. Using these conditions, the maximum removal efficiency predicted for the desert soil, coastal soil and clay soil (Fig. 4.22) are 98.67, 97.57% and 76.85%, respectively at optimal concentrations 0.98 vol% of APG and 0.8 mg/l of Fe^0. The optimized parameter is validated by performing experiments with the optimized input parameters. The experimental results showed a diesel removal efficiency of 98.3, 97.2, and 75.9% for desert soil, coastal soil, and clay soil, respectively. The closeness of the results with optimized parameter exhibits the suitability and accuracy of the developed model.

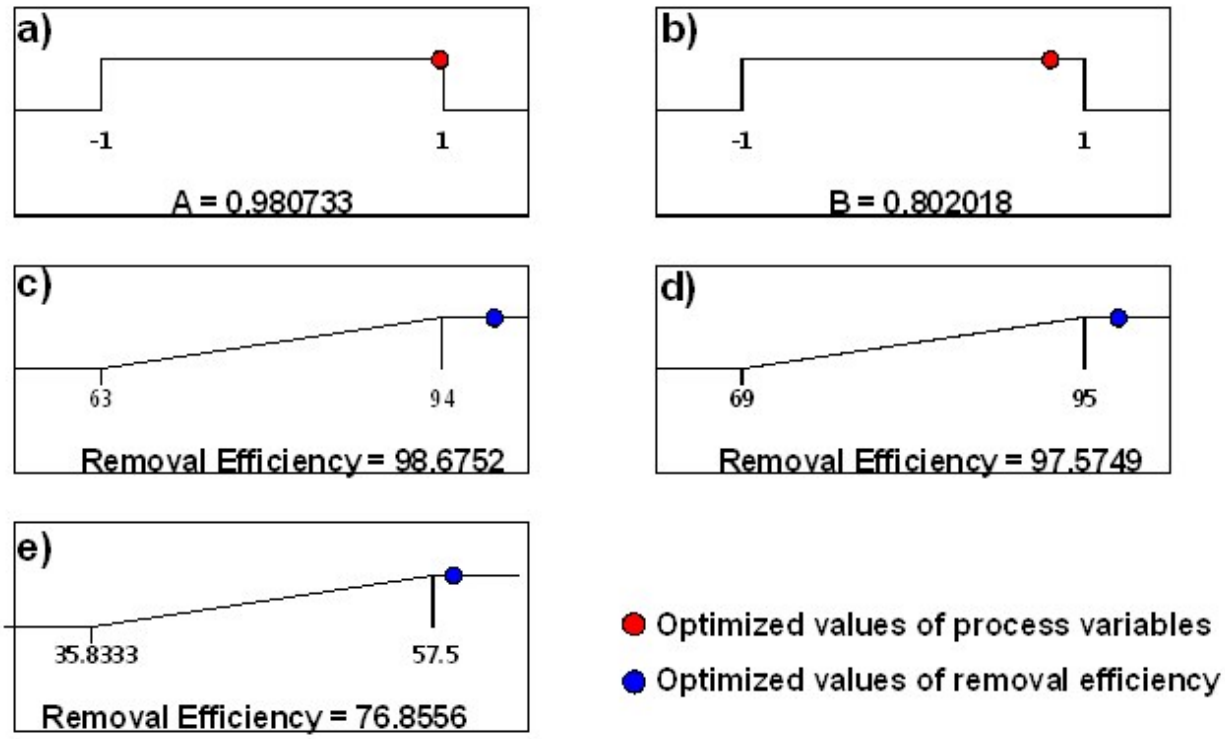

Fig. 4.22 Ramps of the numerical optimization of process variables APG-Ph concentration (a) and Fe^0 concentration (b) to maximize the targeted response, diesel removal efficiency from (c) desert soil (d) coastal soil and (e) clay soil.

4.2 Discussion (soil remediation)

Remediation of diesel contaminated soil by Tween-80 and SDS foam stabilized with Allyl alcohol and Ethylene glycol

Ethylene glycol results in reduction of foamability and foam stability with an increase in surface tension values, in contrast, allyl alcohol produces an enhanced foam behavior showing decrease in surface tension with increase in concentartions due to the positive and negative synergistic effect of the surfactant with different additives (Sidim and Acar, 2013). The increase in surface tension with increase in ethylene glycol concentration can be explained based on the stronger interaction between its hydroxyl group and the hydrophobic part of the surfactant. As the interaction becomes stronger with the hydrophobic group (tail) of surfactant, the availability of surfactant on the gas liquid interface decreases thereby leading to increase in surface tension. This as a whole results in formation of bubbles with weaker film stability. Whereas, the allyl alcohol results in formation of stronger interaction between its hydroxyl group and the hydrophilic portion of the surfactant. Which leads to the formation of strong film between the bubble surfaces, aids in the prevention of foam collapse, and results in highly stable foam (Holmberg et al., 2002). Moreover, it is clear from Fig. 4.4 that the foam stabilized by allyl alcohol enhances the contaminated soil remediation in comparison to that of ethylene glycol stabilized foam, with increases in their concentrations. Furthermore, allyl alcohol addition to nonionic surfactant (Tween-80) brings about higher diesel oil removal efficiency from the contaminated soil than that of anionic surfactant (SDS). This is because Tween 80 being a nonionic surfactant has no charge in its hydrophilic part. Hence, the adsorption of Tween 80 is less onto the soil; most of its molecules remain in the solution and thereby help in the mobilization mechanism of recovery of diesel oil, which is trapped in the soil, due to capillary

action. Whereas, in case of anionic surfactant SDS, the hydrophilic part is negatively charged which makes SDS adsorb onto soil more and reduces the availability of surfactant to remove diesel oil. Thus, a reduced percentage of diesel removal is found in the case of SDS.

Remediation of diesel contaminated soil by Tween-20 foam stabilized with silica nanoparticle

Foaming power of any surfactant solution is represented by foamability. In the current work the foaming power is characterized by Maximum Foam Volume (MFV) which represents the total volume of foam produced by surfactant solution after passing air for 12s (Zhang et al., 2008). The increase in foamability and foam stability with increasing surfactant concentration and the addition of SiO_2 nanoparticle can be elucidated with relation to the retaining of liquid by nanoparticle and hence preventing the foam collapse. As the concentration of surfactant increases the surfactant molecules tends to adsorb on to surface of gas-liquid interface and enhances the formation of bubbles hence the enhanced foamability. At higher concentration of surface active molecules the reduction of surface tension is seen which clearly implies that there is always some surface active molecules left at the gas-liquid interface leading to adsorption of nanoparticles. Significant amount of surfactant remaining in the solution aids in foaming process along with SiO_2 nanoparticle in the dispersion (Lesov et al., 2014; Sun et al., 2014).

Now, it can be seen from the Fig. 4.5 that the surface tension of 5 mg/l hydrophobic SiO_2 dispersion is much lower than that of 5 mg/l hydrophilic SiO_2dispersion and Tween-20 solution (Bera et al., 2013). Also, evidently the hydrophobic SiO_2 nanoparticle produces higher foamability and foam stability compared to the hydrophilic SiO_2 nanoparticle and there is a valid reason to this fact. The surface hydrophobicity places a major role in foaming behavior of surfactant and nanoparticle systems (Kelly and Spottiswood, 1982). The hydrophobic SiO_2

nanoparticles tend to decrease surface tension (Fig. 4.5) by strongly adhering at the gas-liquid interface. With more hydrophobic particles attached to the interface the increased foamability can be explained by the increased stability of thin foam films (Morris et al., 2014; Vijayaraghavan et al., 2006). This inter particle interaction at the gas-liquid interface increases the thin foam film stability which in turn prevents the coalescence or breakage of bubbles (Osei-Bonsu et al., 2015; Stocco et al., 2009). Also, the particles retained at the gas-liquid interface restrict the liquid drainage from the thin foam film (Zhang et al., 2013).

Remediation of diesel contaminated soil by APG-Ph foam stabilized with iron and oxide nanopowders

Foam treatment process requires less quantity of surfactant compared to that of the surfactant solution flushing technique (Maire et al., 2015). Contaminated soil treated only with an aqueous dispersion of Fe^0 requires 6.6 kg of Fe^0 per cubic meter of land surface, whereas, delivered along with foam, requires mere 0.053 kg of Fe^0 per cubic meter of land (Srirattana et al., 2017).

In the present study, soils are contaminated at diesel loading of ~ 83 g diesel/kg soil, and the maximum 94.3, 95.6 and 57.5 % diesel removal is achieved from contaminated desert soil, coastal soil and clay soil, respectively, by using nano Fe^0 (3.5 mg/l) stabilized foam. This is comparable with or better than the results obtained by using other conventional methods (Chagas-Spinelli et al., 2012; Godoy-Faundez et al., 2007; Silva-Castro et al., 2012). (Chagas-Spinelli et al., 2012) study bioremediation of clay soil contaminated with diesel loading of 40 g diesel/kg soil. 87% degradation of diesel after 129 days of treatment with a mixed bacterial consortium comprising of *Acinetobacter*, *Arthrobacter*, *Bacillus*, *Paenibacillus*, *Pseudomonas,* and *Staphylococcus* has been reported. Silva-Castro et al. (2012) achieve 51% degradation of diesel from clay soil, which is initially contaminated with 20 g diesel/kg of soil, by utilizing

heterotrophic bacteria along with biostimulating agent. Tsai et al. (2010) use H_2O_2, and Fe_3O_4 assisted Fenton oxidation process and reported 27% removal of diesel from contaminated clayey soil after 60 days of treatment. The soil is initially contaminated at the rate of 10 g diesel/kg soil.

To date, very few studies report on the treatment of diesel-contaminated desert and coastal soils by using conventional methods (Al-Kindi and Abed, 2016; Balba et al., 1998). Godoy-Faundez et al. (2007) report the treatment of Atacama desert soil, initially contaminated with 50 to 250 g diesel per kg of soil, by bio composting method. 60 % of diesel removal is reported after 56 days of treatment, with sawdust as a composting agent. Bento et al. (2005) investigate microbial biodegradation of diesel-contaminated coastal soil loaded with 28 g of diesel per kg of soil. Treatment of the polluted soil with hydrocarbon degrading microbes results in 72.7 % of diesel removal from the soil.

Effect of nanoparticles

The increase in foamability and foam stability can be explained in terms of retention of high amount liquid by nanoparticles (up to concentration 3.5 mg/l) and thereby preventing the foam breakage (Blanco et al., 2013). To achieve this, the nanoparticles have to remain on the surface of the liquid film of foam. The strong adsorption of the nanoparticles on the hydrophilic part of the surfactant molecule aids in enhancing foamability and foam stability (Yazhgur et al., 2013a) and decreasing surface tension (Su et al., 2014). The presence of iron or iron oxide particles in the dispersion enhances the adsorption of surfactant on the solid (nanoparticles)-liquid interface, which in turn increases the repulsive electrostatic force existing between the particles and the surrounding liquid and thus reduces the surface tension (Harikrishnan et al., 2017). Obviously, more stable nanoparticle dispersion as indicated in ξ potential results (Fig. 4.13) helps to enhance foam stability.

A clear negative synergy between the nanoparticle concentration and foamability, foam stability, and surface tension is developed at higher nanoparticle concentrations (Fig. 4.11 for 4 and 5 mg/l). One possible explanation could be that the increase in nanoparticle concentration above the threshold value (3.5 mg/l) attracts too many surfactant molecules towards the solid-liquid interface rather than the gas-liquid interface. As a result, the density of the surfactant molecule at the gas-liquid interface decreases. Thus, the strength of the cohesive force necessary to exert between the surfactant molecules at the gas-liquid interface to retain the foam structure diminishes, and the structure collapses (Blanco et al., 2013). Additionally, an increase in the concentration of nanoparticles reduces the space between the neighboring surfactant molecules, which exhibits an attractive Van der Waals force rather than the repulsive electrostatic force and thereby increases the surface tension (Bhuiyan et al., 2015).

For effective remediation, the foam has to flow through the soil, desorb the diesel contaminants from the surface of the soil (by reducing surface tension between soil and contaminant) and carry it along with, leaving the soil free of pollutant (Couto et al., 2009). Solubilization and mobilization are considered to be the two major mechanisms involved in the removal of diesel oil from contaminated soil (Javanbakht and Goual, 2016). Solubilization occurs above the critical micelle concentration (CMC), where surfactants molecules solubilize the contaminants by the formation of micelles (Jawitz et al., 1998). Mobilization occurs at a concentration below the CMC (Vreysen and Maes, 2005). In this study, as the surfactant concentration does not reach the critical micelle concentration (540 mgL^{-1}) (Vreysen and Maes, 2005), it can be inferred that the mobilization mechanism is predominant. The decrease in the surface tension of the nanoparticle dispersed aqueous surfactant solution with an increase in its respective concentration supports the mobilization of diesel oil from the contaminated soil, as

observed from Fig. 4.12. The slight increase in viscosity of the surfactant foam with nanoparticles probably helps the foam stability, which is important to penetrate the contaminated soil surface (unsaturated porous media) (Zhao et al., 2016b). This is also in agreement with the results reported in literature. Kadoi and Nakae, (2011) state that the high viscous solution produces highly stable foam and results in the prevention of bubble breakage and drainage of liquid from the foam. The foam penetration and successful displacement of the contaminants in the soil surface are majorly described by the longevity of foam in the porous media (Osei-Bonsu et al., 2017b).

The zero-valent iron nanoparticle has been widely used in different environmental applications owing to its reduced size, enhanced mobility in the zone of contamination and high reactivity with the hazardous hydrocarbon-related pollutants (Guo et al., 2015; Hou et al., 2009). Although the stable forms of iron in nature are Fe^{2+} and Fe^{3+}, it is possible to synthesize Fe^0. Fe^0 has a strong reducing tendency, itself converting to oxide. The presence of metallic Fe^0 within the core of nanoparticles (even if the surface gets slightly oxidized during preparation) slowly oxidizes to release electron pairs, which in turn react with the organic contaminants and transform/decay these (Raychoudhury and Scheytt, 2013). This could explain the higher activity of Fe^0 compared to the Fe_3O_4 nanoparticle, although Fe_3O_4 has a smaller particle size and larger surface area. Some reduction of Pb and As related pollutants are observed in the soils treated with nanoparticle stabilized foams (Table 4.3). While both Fe^0 or Fe_3O_4 can react with arsenic compound (depending on the oxidation state of arsenic), stronger adsorption affinity of the arsenic compound towards Fe_3O_4 nanoparticle might be more helpful in removal of the toxic chemical from the soil, as suggested by the results (Yan et al., 2012). Strong adsorption of lead on Fe^0 could be responsible for reducing lead in the desert soil (Mar Gil-Díaz et al., 2014).

Effect of Soil Properties

It is a well known fact that the texture of soil influences the binding of contaminants on the soil as well as its removal from the soil. The sandy soil with a larger particle size (0.425-2 mm) has a smaller surface area, and on the other hand, clay soil with a smaller particle size (< 0.002 mm) has a larger surface area (Takahashi, 1996). Therefore, it is expected that the clay soil would adsorb more contaminants on the surface compared to desert or coastal soils. In a similar vein, cation exchange through adsorption is favored by the larger cation if two atoms have the same valence, which is mostly true for the heavy metal contaminants (Sassman and Lee, 2005).

The clay soil with small particle size generally has higher porosity and demonstrate higher water holding capacity than that of the sandy soil (Dexter, 2004). The clay soil studied in the present work has the highest porosity of 68.7%, whereas desert soil and coastal soil show porosity of 42.5 and 37.5 %, respectively as mentioned in Table 3.1. Presumably, deep penetration and strong binding of the contaminants in clay soil are expected compared to those in the desert soil and coastal soil (Abdel-Moghny et al., 2012b). Hence, it becomes difficult to remove these strongly adhered contaminants from clay. The strongly bound contaminant might reduce the wettability of the clay soil by an aqueous solution. As a result, flushing of the contaminated soil by aqueous foam becomes difficult (Fogden, 2012). The organic matter present in the soil adsorbs diesel contaminant onto it strongly and decreases the diesel removal efficiency during any treatment process (Yen et al., 2011). Here, the clay soil has the maximum organic matter (3.96%) bound on it.

The activation energy exerted by the soil to bind contaminants on the surface depends on its nature (Li et al., 2015). Sandy soil requires lower activation energy, while clayey soil requires higher activation energy. Binding of contaminant on clay soil occurs by strong van der Waals

force, hydrogen bond or hydrophobic bond. As a result, the contaminant entraps on the soil layer, and this makes the remediation of clay soil a more difficult process (Johannes van Duijn et al., 2007; Ming et al., 2015). Moreover, due to an interaction with the organophilic phase of the adsorbed contaminants, the clay soil tends to swell and blocks the pores available for surfactant interaction (Li et al., 2016). The swollen clay restricts the flow of foam through the pores, and removal of contaminants from clay soil becomes difficult (Aksu et al., 2015). The clay soil reported in the present study contains some Ca^{2+} (0.78 wt. %), which decreases to 0.49 and 0.4 wt. % after treatment with Fe^0 and Fe_3O_4 nanoparticle stabilized foam, respectively. Similarly, the amount of Mg^{2+} (1.29 wt. %) present in clay soil originally, decreases to 0.94 and 0.89 wt. % after treatment with Fe^0 and Fe_3O_4 nanoparticle stabilized foam, respectively, as mentioned in Table 4.3. During the treatment process, this release of Ca^{2+} and Mg^{2+} from the soil into the solution could result in a complex precipitate of the surfactant. This complex precipitate, in turn, may settle in the soil pores, thereby causing severe pore clogging in clay soil, which could be another cause of low diesel removal from the soil. Thus, sandy soil is easier to remediate by surfactant foam treatment process than clay soil (Zuo et al., 2015). Results indicate that the physical and chemical properties of nanoparticles and soil texture could play critical roles in soil remediation. The effects of different sizes of these nanoparticles in stabilizing foams and on remediation of diesel-contaminated soil have to be investigated in the near future.

Comparison of different surfactant systems for desert soil remediation

The soil remediation results have shown that the diesel removal efficiency decreases in the following order APG-Ph/Fe^0 > APG-Ph/Fe_3O_4 > Tween-20/SiO_2 > Tween-80/allyl alcohol. The results are in agreement with that of existing literature (Dass et al., 2015;Torres et al., 2005). The Tween-80 having higher ionic strength than Tween-20 is expected to produce higher removal efficiency, as reported by others also. Torres et al. (2005) show 14.5 and 13.4 % removal efficiency of crude oil from sandy soil by utilizing aqueous solution of Tween-80 and Tween-20, respectively. The major reason of the contradictory result probably lies with the interplay between the surfactant and SiO_2 nanoparticle. The SiO_2 nanoparticle is able to stabilize the foam compared to the biodegradable additive allyl alcohol.

The glucose based nonionic surfactant APG-Ph having shorter alkyl chain length (C8) has lower adsorption rate on soil and hence it is able to detach more contaminant from soil and produces higher diesel removal efficiency. Whereas, the nonionic surfactants Tween-20 (C12) and Tween 80 (C18) having longer alkyl chain length and higher adsorption is unable to detach the contaminant to great extent and hence produces lower removal efficiency (Iglauer et al., 2004). On comparing the effect of nanoparticle on diesel removal efficiency the Fe^0 achieves better results than that of SiO_2. The causes could be: The bigger particle size of SiO_2, 55 nm, whereas, the particle size of Fe^0 reported in the study is 20 nm. Thus the smaller particle size aids in better stabilization of foam as well as to achieve higher contaminant removal efficiency. In addition, Fe^0 may act as a strong reducing agent by donating electron from the iron to the contaminants bound on to the soil surface (itself converting to oxide) effectively degrading the contaminant (Bruton et al., 2015).

Optimization using RSM

The dosage of Fe^0 is a predominant factor in the removal of the contaminant from the soil. The reactive nature of Fe^0 aids in better removal of contaminants from soil. Also, the success in obtaining maximum diesel removal from coastal soil is exhibited by the synergistic interactions between the two independent variables APG-Ph and Fe^0 concentrations. Optimization of these parameters yields an optimum condition of 0.98 vol% APG-Ph and 0.8 mg/l Fe^0 concentrations to achieve maximum desirable removal efficiency. Considering the previous reported results, the obtained optimum condition produces better results. Previously, Gharibzadeh et al. 2018) are able to produce mere 66.6% removal efficiency from contaminated sandy soil at optimum surfactant concentration of 5000 mgL^{-1}, but in the current study we are able to achieve a maximum of around 98.7 % of diesel removal efficiency from contaminated soil. Also this removal efficiency reported here is achieved at a minimal concentration of surfactant (0.98 vol%) as the treatment involves the application of foam rather surfactant solution.

4.3 Formulation of liquid laundry detergents

Foam behavior is an important aspect of detergent products. The detergent must possess good foaming capabilities, regardless of the quality of water used for washing the fabric. Foam properties of the prepared detergent formulations in different hardness levels of water have been described. Foamability and foam stability are important factors for quantifying the foaming phenomenon of the detergent system (Sakai and Kaneko, 2004). Further explanation of properties of foam such as foamability, foam stability, and foam drainage has been attempted here.

4.3.1 Characteristics of the prepared liquid laundry detergents

Foamability

Foamability indicates the foaming power of any aqueous system of surfactant. The foamability is represented as MFV, which shows the maximum volume of foam generated by the detergent formulation. It is important to study the influence of hardness of the water in detergent properties. The comparison of the MFV, produced by the different detergent formulations (S1 and S2) in different hardness levels of water is shown in Fig. 4.23. The detergent formulation showed maximum foamability in hypersaline water as the excess salt induces the surfactants to produce foamability and foam stability. The ions present in the salt reduce the electrostatic repulsion of polar head groups of the surfactant and enhance the adsorption of more amount surfactant at the gas-liquid interface. As more surfactant accumulates at the gas-liquid interface the bubble film tends be more stable (Varade and Ghosh, 2017). The detergent formulation S1.8 with combination of anionic and nonionic surfactant showed maximum foam volume 101.1 mL in hypersaline water. The formulation S1.1 having anionic surfactant 4 wt% of SLS alone shows the least foamability of 88.2 mL in RO water. Overall the maximum foamability is achieved by

the formulation S2.1, producing a foam volume of 148.8 followed by S2.7 with foam volume of 140 mL in hypersaline water. S2.1 having anionic surfactant SLS alone at 10 wt% shows maximum foamability. Thus anionic surfactant is able to produce higher foamability at higher concentrations as well as it is effective in hypersaline water. Using nonionic surfactant APG (S2.3) help us to achieve better foamability in hard water (112.8 mL).

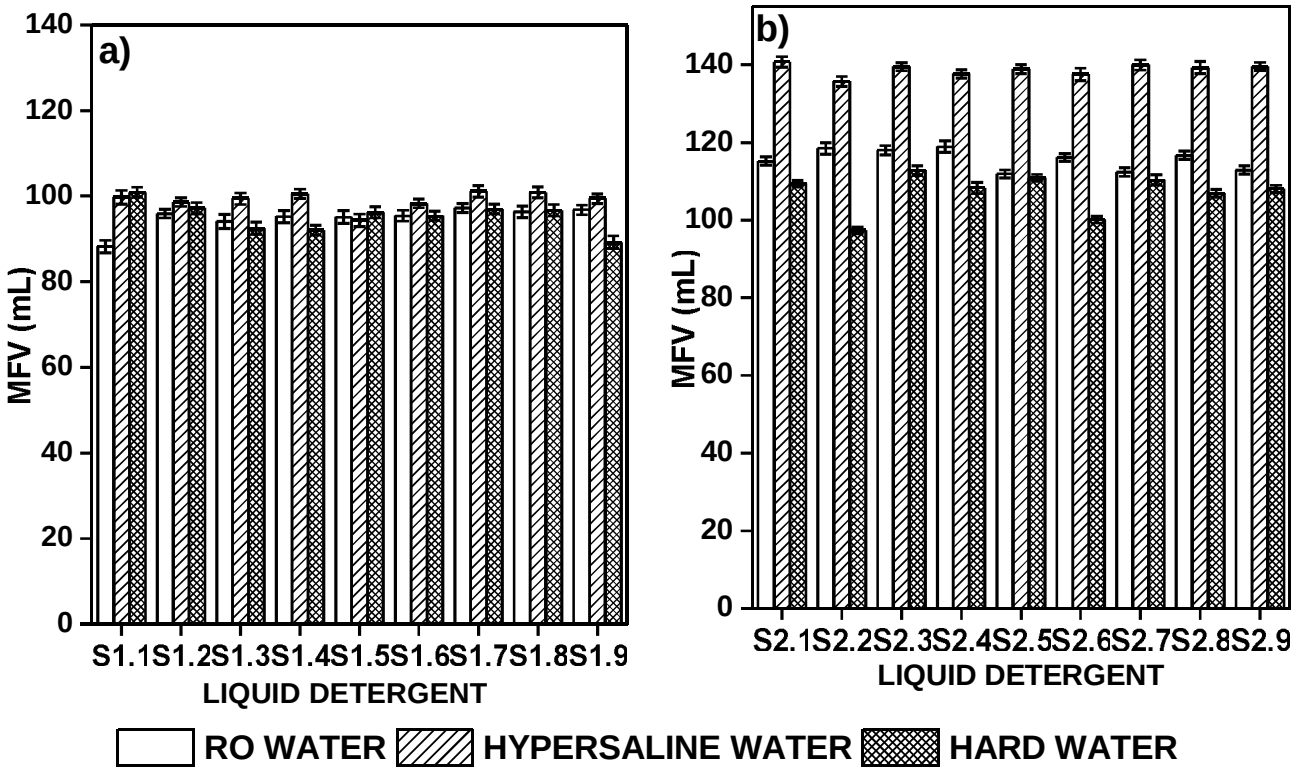

Fig. 4.23 Comparison of Maximum foam volume (MFV) for the detergent formulations in different water hardness levels. a) and b) Maximum foam volume generated using liquid detergent formulations S1 and S2 respectively.

Foam stability

The foam stability of the prepared detergent formulations is represented as RMI 30 (Tamura et al., 1999). RMI 30 is the volume of foam present after 30 s of foam collapse (Wang et al., 2014). Fig. 4.24 displays the comparison of the stability of foam using different detergent formulations. The foam is found to be stable in hypersaline water for both sets of formulations.

The formulation consisting of SLS, Tween-20, and Tween-80 displayed lower foam stability in hard water. The formulation containing only Tween-20 (Formulation no S1.2) shows the highest foam stability of 94.8 mL in RO water, amongst the first set of formulations (S1). Similarly, the formulation S2.9 containing combination of anionic and nonionic surfactant shows maximum foam stability of 139.2 mL in hyper saline water among the second set of detergent formulations (S2). The combination of nonionic surfactants Triton X-100 and APG (S2.6) yielded better foam stability (112.9 mL) in hard water.

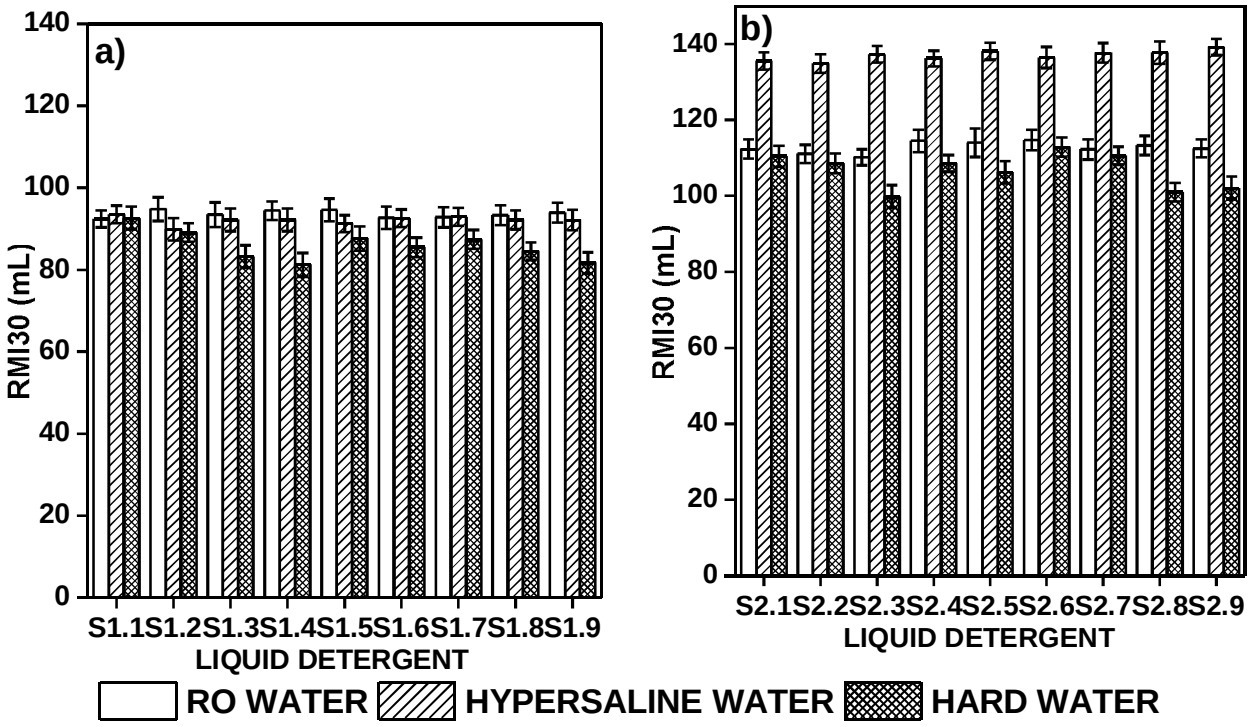

Fig. 4.24 Foam stability represented as Ross Miles Index (RMI 30) in various hardness levels of water. a) & b) represents the foam stability of liquid detergent formulation sets S1 and S2 respectively.

Surface Tension (σ)

It is important to formulate a detergent which provides better cleaning efficiency with a reduction in surface tension value (Meshram et al., 2015). The surface tension values of all the prepared liquid detergent formulations are shown in Table 4.7. The detergent formulation prepared with SLS, Triton X-100 and APG had lower surface tension values in the range of 20.5 to 23.3 dynes/cm. The highest surface tension of 23.1 is seen among the second set of detergent formulation is S2.2 which has only nonionic surfactant Triton X-100. The least surface tension 20.5 dynes/cm is achieved in case of S2.1 which is prepared with 10 wt% of anionic surfactant SLS alone. The other set of formulations (S1) prepared with SLS and Tween system shows a higher surface tension in the range of 26.3 to 38.7 dynes/cm. Especially the formulation containing nonionic Tween-80 alone (S1.3) results in maximum surface tension of 38.7 dynes/cm when compared to other formulations containing a mixed surfactant.

Table 4.7: Surface tension (σ) values of detergent formulations prepared with SLS, Tween-20 and Tween-80 (S1) and SLS, Triton X-100 and APG (S2).

Formulation	Surface tension (dynes/cm)	Formulation	Surface tension (dynes/cm)
S1.1	27.2	S2.1	20.4
S1.2	38.4	S2.2	23.1
S1.3	38.6	S2.3	20.7
S1.4	27.0	S2.4	21.3
S1.5	28.9	S2.5	21.8
S1.6	36.4	S2.6	23.3
S1.7	26.2	S2.7	21.4
S1.8	28.7	S2.8	20.5
S1.9	27.6	S2.9	21.7

Quantification of detergency

The performance of different liquid detergent formulations on cotton and woolen fabric soiled with oily soil and grease is reported in Fig. 4.25. Removal of oily soil determines the detergency, and the enhancement of detergency is possible when enough surfactant concentration adsorbs on the layer of soil and eliminates it. The formulations containing SLS and Tween-20 or Tween-80 show detergency in the range 40-50%. This is the maximum detergency when the cotton fabric is used. It is much lesser in case of woolen fabric. This is because the surfactant combination of SLS and Tween is less adsorbed to the soil to solubilize the oily soil and hence the less detergency. Also, the maximum detergency is exhibited by the formulation no S1.2 where Tween-20 is only present. The detergency could also be correlated to the foam behavior as the set of formulations S2 produces maximum foamability and foam stability (Jadidi et al., 2013). The detergency % of formulation set S2 is noticed to be much higher in treating both woolen and cotton fabrics. The maximum detergency of 90% and 89% in treating cotton and the woolen fabric is observed, respectively, for formulation S2.9. The presence of all three surfactants SLS, Triton X-100, and APG in formulation no S2.9, lead to a synergistic effect thereby enhancing the detergency.

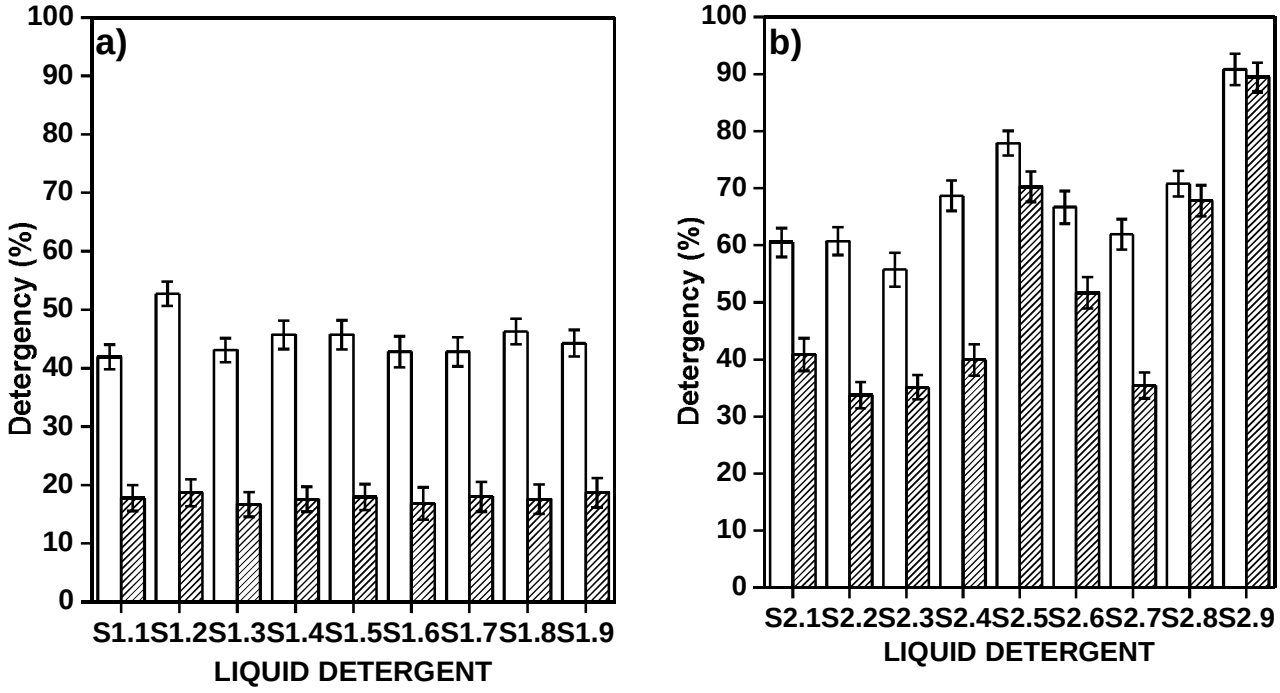

Fig. 4.25 a) & b) Performance of the prepared liquid detergent formulations in the removal of soil from cotton ☐ and woolen fabrics ▨

Fabric surface characteristics

The potential impact of the formulation with maximum detergency (formulation no S2.9) on fabric quality is further probed by studying the surface morphology of the fabric used in the study.

Scanning Electron Microscopy images show the presence of oily soil on the surface of cotton (Fig. 4.26 (a)) and woolen fabric (Fig. 4.26 (b)). After washing, the oily soil is removed, and due to the presence of polymer PVP, there is no redeposition of oily soil onto the fabric. Analysis of the surface morphology of the fabric is also helpful in studying the durability of the fabric subjected to laundry detergents. As it is seen that there is no crack or deformation on the surface of fabric after washing (Refer to Fig. 4.26 (c) and (d), hence it is concluded that the prepared liquid detergent formulation would not hamper the fabric quality.

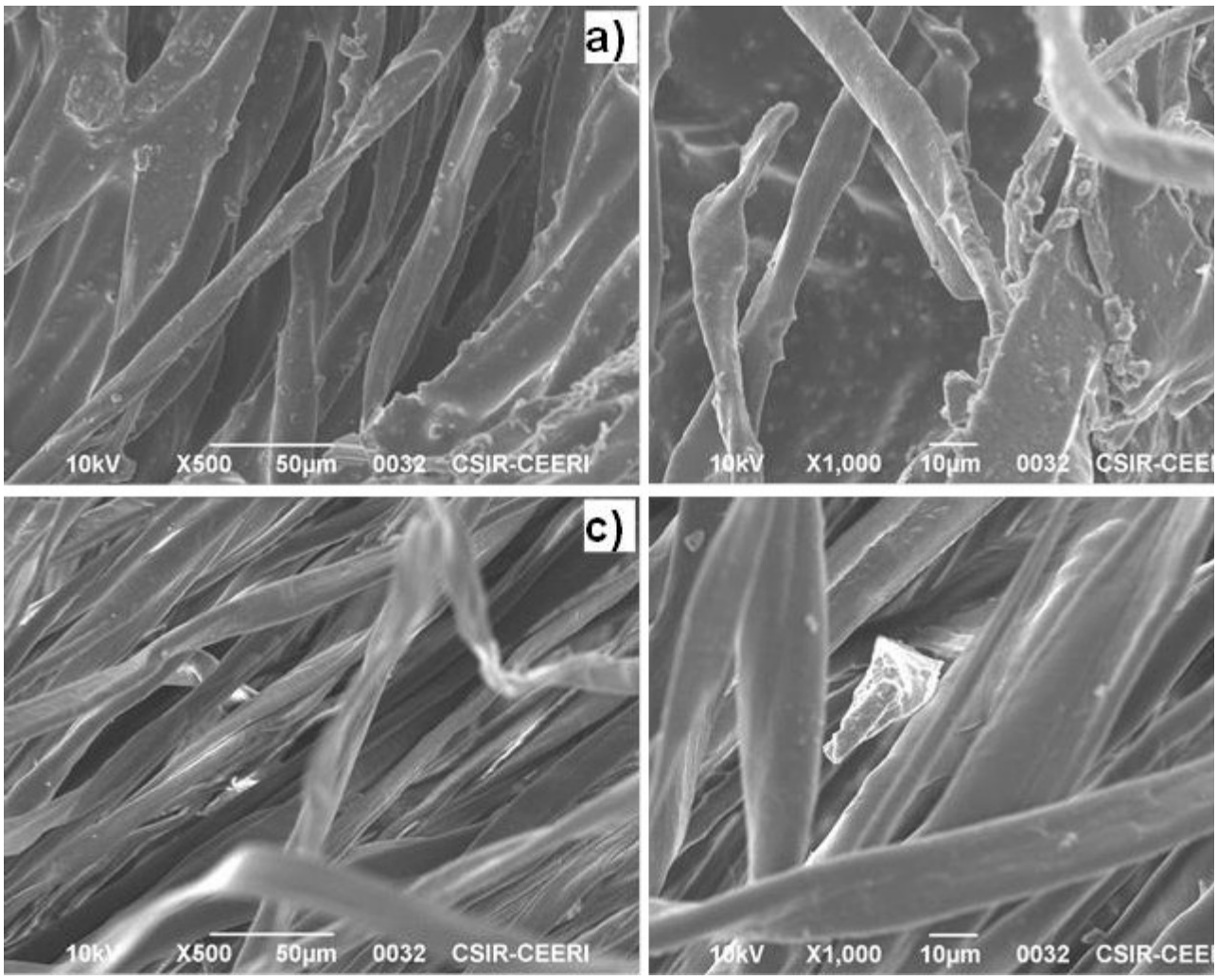

Fig. 4.26 Scanning Electron Micrographs of fabric fibers. a) and b) Depicts the cotton and woolen cloth soiled with oily soil prior to washing respectively. c) and d) Fiber surface of cotton and woolen cloth after washing with formulation S2.9.

4.4 Discussion (Laundry detergent)

Due to the presence of a charge on the surface of the micelle structure, all the prepared detergent formulations produce higher maximum volume of foam in hypersaline water. Also, the formulations S2.1-S2.9 (SET-2) produced MFV more than 100 mL, even in hard water. Thus, the formulations (SET-2) are believed to have the potential to produce better detergency for any hardness level of water. The higher viscosity of Tween-20 surfactant leads to higher foam stability. Whereas, the second set of formulations (S2) containing a combination of SLS, Triton X-100, and APG the foam is found to be much more stable in all types of water. The higher foam stability could be correlated with the lesser surface tension exhibited by these formulations. Thus, the second set of detergent formulations (S2) could achieve better performance in terms of foamability and foam stability, regardless of the water hardness level. The combinations of nonionic surfactant help to produce higher foam behavior in hard water. Surface tension directly affects the detergency as it is seen from Fig. 4.25 that the set 1 (S1) formulations having higher surface tension show reduced detergency, whereas, the other formulation set (S2) with lower surface tension has better detergency. This is in accordance with the well-established results in the literature (Savarino et al., 2009). The better performance of detergent (S2.9) can attributed to the mixture of surfactant and the interaction of hydrophilic and hydrophobic of the amphiphilic surfactant structure (Polarz et al., 2018). The formation of aggregates and the adsorption of surfactants on the gas-liquid interface are the characteristic properties of surfactants, which are determined by the length of its hydrophobic chain (Somasundaran and Huang, 2001; Zana, 1996). However, as we can see from the surface tension results, the detergent formulation containing mixture of anionic and nonionic surfactants shows better detergency behavior because of a significant reduction in surface tension. It is due to the reason that the hydrophilic head

group of anionic surfactant SLS is located further than the polar head group of nonionic surfactant, and hence the repulsion energy between the charged groups is lesser (Pejic, 2016).